

# Dynamics of Polymer Chains in Poly(ethylene oxide) / Silica Nanocomposites via a Combined Computational and Experimental Approach\*

*Albert J. Power,<sup>1,2</sup> Hellen Papananou,<sup>3,4</sup> Anastassia N. Rissanou,<sup>1,5</sup> Massimiliano Labardi,<sup>6</sup>  
Kiriaki Chrissopoulou,<sup>3,\*</sup> Vagelis Harmandaris<sup>1,2,5,\*</sup> and Spiros H. Anastasiadis<sup>3,4,\*</sup>*

<sup>1</sup> Department of Mathematics & Applied Mathematics, University of Crete, 70013 Heraklion Crete, Greece

<sup>2</sup> Institute of Applied and Computational Mathematics, Foundation for Research and Technology-Hellas, 700 13 Heraklion Crete, Greece

<sup>3</sup> Institute of Electronic Structure and Laser, Foundation for Research and Technology-Hellas, 700 13 Heraklion Crete, Greece

<sup>4</sup> Department of Chemistry, University of Crete, P.O. Box 2208, 710 03 Heraklion Crete, Greece

<sup>5</sup> Computation-based Science and Technology Research Center, The Cyprus Institute, 2121 Nicosia, Cyprus

<sup>6</sup> CNR-IPCF, c/o Physics Department, University of Pisa, Largo Pontecorvo 3, 56127 Pisa, Italy

---

\* This manuscript is dedicated to Doros N. Theodorou on the occasion of his 65<sup>th</sup> birthday

## Abstract

The dynamics of polymer chains in poly(ethylene oxide) / silica nanoparticles, PEO / SiO<sub>2</sub>, nanohybrids has been investigated via a combined computational and experimental approach that involves atomistic molecular dynamics simulations and dielectric relaxation spectroscopy (DRS) measurements. The complementarity of the approaches allows us to study systems with different polymer molecular weights, nanoparticle radii and compositions across a broad range of temperatures. We study the effect of spatial confinement, induced by the nanoparticles, and of chain adsorption on the polymer structure and dynamics. Investigation of the static properties of the nanocomposites via detailed atomistic simulations reveals a heterogeneous polymer density layer at the vicinity of the PEO/SiO<sub>2</sub> interface, which exhibits an intense maximum close to the inorganic surface with the bulk density reached for distances  $\sim 1-1.2$ nm away from the nanoparticle. For small volume fraction of nanoparticles, the polymer dynamics, probed by the atomistic simulations of low molecular weight chains at high temperatures, is consistent with the presence of a thin adsorbed layer that shows slow dynamics with the dynamics far away from the nanoparticle being similar to that in the bulk. However, for high volume fraction of nanoparticles (strong confinement) the dynamics of all polymer chains are predicted slower than that in the bulk. On the other hand, the experimental findings, for high molecular weight systems measured at temperatures below the melting temperature of the polymer, probed by DRS, similar dynamics both for the local  $\beta$ -process and the segmental dynamics. These differences can be attributed to various parameters: systems of different molecular weight and nanoparticle state of dispersion, the different temperature range studied by the different methods, the potential presence of a reduced mobility PEO/SiO<sub>2</sub> interfacial layer that doesn't contribute to the dielectric spectrum, as well as to the presence of amorphous/crystalline interfaces in the experimental samples that may lead to a different dynamical behavior of the PEO chains.

**Keywords:** polymer nanocomposites, segmental relaxation, confinement, chain adsorption, atomistic simulations, dielectric relaxation spectroscopy, polyethylene oxide, silica

## 1. Introduction

The investigation of the structure, chain conformation and dynamics in polymer nanocomposites (PNCs) constitutes a very active research area due to the innovative properties of these materials that make them candidates for a broad range of applications.<sup>1-12</sup> The properties of polymer chains are different close to the surface of a nanoadditive or under confinement, when compared to those in the bulk, affecting the overall behavior of the systems.<sup>13-25</sup> Important advances both in basic research<sup>2,4,6,11,26,27</sup> and in different industrial fields have been made on hybrid polymer/nanoparticle systems.<sup>28-30</sup> Moreover, a number of computational<sup>4,31-48</sup>, experimental<sup>17-19,21,22,24,26,27,49-59</sup> or combined studies<sup>13,60</sup> have been employed to investigate the effects of the presence of the interfaces on the properties of the polymer providing a measure of the interphase length.<sup>13,15,34,47,61-65</sup>

A special case of nanohybrids is the one composed of silica nanoparticles (NPs), SiO<sub>2</sub>, dispersed in a polymer matrix. Silica nanoparticles are of great interest due to their excellent properties and the range of their applications in many scientific fields. Their high chemical stability,<sup>66</sup> attributed to the Si-O bond, is important for applications as drug delivery systems.<sup>67,68</sup> Moreover their excellent biocompatibility,<sup>69</sup> heat resistance,<sup>70</sup> low toxicity,<sup>71</sup> simple synthetic approach,<sup>72</sup> and massive synthetic supply<sup>73</sup> render them attractive for biological applications,<sup>66,74</sup> like cell tracing,<sup>75</sup> biosensing<sup>76</sup> and as diagnostic tools.<sup>77</sup> Extensive applications of silica nanoparticles are also found in rubber technology, where they are used to improve the properties of tires and other rubber materials.<sup>14,78</sup>

Poly(ethylene oxide), PEO, is a widely used polymer in many technological applications.<sup>79</sup> It is hydrophilic, biocompatible and it possesses high ion transport properties; therefore, it is suitable for many fields of research including biomaterials, drug-delivery and solid state polymer electrolytes.<sup>80-84</sup> PEO is the most frequently studied polymer ionic conductor; however, its high crystallinity prevents its further utilization. Different additives can be used to suppress its crystallization and, thus, its nanohybrids can be utilized as promising materials for applications in solid-state lithium batteries.<sup>85</sup> Specific attractive interactions exist between PEO and silica nanoparticles, mainly attributed to the formation of hydrogen bonds, which force polymer chains to adsorb onto the surface of the nanoparticle<sup>86,87</sup>, resulting in the stabilization of the systems.<sup>13,17,26,27,47,88</sup> Numerous pharmaceutical and industrial applications have been reported for such nanocomposite systems.<sup>89-92</sup>

The properties of PEO/SiO<sub>2</sub> nanocomposites have been investigated utilizing various simulation models<sup>32,47,48,93</sup> and experimental techniques<sup>49,53,57,94-96</sup>. In a previous work, we have investigated the structural and conformational properties of PEO chains of various molecular weights in PEO/SiO<sub>2</sub> nanocomposites as a function of temperature and degree of confinement<sup>13</sup>. A combined experimental and theoretical approach revealed that spatial confinement affects significantly the conformational behavior of polymer chains causing an important increase of the *gauche* conformations in comparison to the neat PEO at the same temperatures. Moreover, the type of end group of the PEO (CH<sub>3</sub> or OH) did not affect the average conformational properties of the simulated polymer chains. The presence of the SiO<sub>2</sub> affects significantly the degree of crystallinity of PEO as well.<sup>17</sup> The degree of confinement that the chains suffer and the curvature of the nanoparticles, which affects the chain adsorption, has been shown to be the two determining factors that can act synergistically and lead to a significant decrease of the crystallinity for nanohybrids with high inorganic content.

Contrary to the conformational properties, which do not seem to depend on the PEO end groups, the dynamics was found to be affected by the type of end-groups with the chains with OH end-groups exhibiting slower translation dynamics within an interphase region of ~2-3 nm close to the nanoparticle surface.<sup>48</sup> Recently, Skountzos, et al.<sup>47</sup> studied nanocomposites of PEO with silica nanoparticles and investigated the effect of the different chain end-group (CH<sub>3</sub> and OH) on the train, loop, and tail conformations of the chains adsorbed on the silica nanoparticle. It was shown that PEO-CH<sub>3</sub> chains adsorb along their entire backbone whereas PEO-OH chains prefer to adsorb mostly by their end-groups (OH). Moreover, PEO-CH<sub>3</sub> chains have faster chain (Rouse) relaxation times near the nanoparticle surface in comparison with the PEO-OH ones, whereas no difference in the dynamics is observed for the free chains away from the nanoparticle. The diffusivity and the arrangement of silica nanoparticles have been also investigated in hybrid systems of silica nanoparticles with either grafted PEO chains or in a matrix of PEO oligomers.<sup>93</sup> Analysis of the dynamics revealed that, at short time scales, grafted chains relax faster than the free chains at low temperatures; however, this behavior is reversed with increasing temperature.

From the experimental point of view, Kim et al.<sup>96</sup> studied the effects of polymer molecular weight, temperature and solvent dilution on polymer dynamics in PEO-silica nanocomposites. They found that the adsorption of PEO segments onto the silica surface produces a polymer layer

of reduced-mobility over a temperature range 343 – 373 K, which is not observed at higher temperatures. Strongly anisotropic segmental mobility was found within this layer compared to a rotation of the backbone. Glomann, et al.<sup>49,95</sup> performed neutron spin echo (NSE) and high resolution time-of-flight (TOF) spectroscopy experiments on PEO/silica nanocomposites with PEO chains with different end groups (OH or CH<sub>3</sub>); in the system with OH end-groups, suppressed translation diffusion was observed, whereas the segmental dynamics was found unaffected, while, in the one with CH<sub>3</sub> end-groups, an adsorbed but not glassy layer was reported possessing fast local dynamics.

Senses, et al.<sup>53,57</sup> studied the nanoparticle dispersion, the polymer conformation as well as the macroscopic and microscopic chain dynamics by applying NSE and neutron backscattering spectroscopy. They found that the Rouse dynamics of the chains slows down with nanoparticle addition and no glassy effect appeared on the adsorbed layer.

From the above short discussion, it is clear that the dynamics of PEO under confinement and/or in the vicinity of inorganic nanoparticles has provided many contradictory results in different studies. Moreover, when PEO formed an intercalated structure between laponite sheets, a significant number of PEO monomer units were found to display a strong slowing down as compared to neat amorphous PEO. This decrease in the segmental mobility was mainly assigned to the complexation of PEO oxygens by the Na<sup>+</sup> counterions located in the laponite interlayer galleries<sup>97</sup>. On the other hand, when PEO was confined between the layers of Na<sup>+</sup>-Montmorillonite, the segmental dynamics was found many orders of magnitude faster than the bulk exhibiting an Arrhenius temperature dependence. In that case, the different behavior was attributed to the severe confinement of the chains.<sup>27</sup> Moreover, no significant effect on the dynamics was detected when PEO was placed within 18 nm diameter Anodic Aluminum Oxide (AAO) pores.<sup>98</sup> When PEO is confined between graphene oxide (GO) layers, the intercalation of polymer chains does not only lead to the suppression of polymer crystallization but also to the suppression of the dielectric  $\alpha$ -relaxation together with a slowing down of the  $\beta$ -relaxation modes.<sup>23</sup> It is, thus, evident that deep understanding of the dynamics of even such an investigated polymer like PEO in its nanocomposites is still missing.

In the current work we present a complementary computational and experimental study of the dynamics in PEO/SiO<sub>2</sub> nanocomposites covering a broad range of molecular length scales. We provide a systematic exploration of the dynamical properties of PEO in the segmental level

through atomistic molecular dynamics (MD) simulations and Dielectric Relaxation Spectroscopy (DRS) experiments. The combined use of the two approaches provides important information in a complementary way. All-atom MD simulations focuses on a detailed analysis in the atomic level, which can capture changes very close to the surface of the nanoparticle, the so-called “bound or dead layer”. On the other hand, Dielectric Spectroscopy can explore different relaxation modes utilizing higher molecular weight PEO. The different resolution of the two methods, as well as the different molecular weights used, result in an exploration of the segmental motion over a broad range of systems and conditions. The effect of the interfacial area is highlighted through a detailed analysis of various measures as a function of the distance from the nanoparticle surface. Different concentrations and molecular weights are investigated by combining the simulation and the experimental findings. The degree of confinement together with the adsorption capacity are found to be the critical parameters for the arrangement of polymer chains at the vicinity of the polymer/silica interface, and, consequently, their mobility.

In the next section the model, the simulation method and the analysis techniques used in the simulations are described together with the neat materials and the nanocomposites that have been investigated experimentally. The results, divided in subsections, are presented in Section 3. Finally, a summary and the conclusions of the current study are presented in Section 4.

## 2. Materials and Methods

### *a. Materials:*

The poly (ethylene oxide), PEO, that was used in the experimental part of this work was purchased from Sigma-Aldrich. It has a molecular weight of 100,000 g/mol and a polydispersity index  $M_w/M_n = 2.4$ . Its melting point is  $T_m=340$  K and its glass transition temperature  $T_g=206$  K. It exhibits a degree of crystallinity of ~65-80% depending on the conditions under which the material is crystallized. From here on, this polymer will be noted as PEO<sub>2270</sub> utilizing its degree of polymerization as subscript. Dynamic Light Scattering, DLS, measurements provided the hydrodynamic radius of PEO<sub>2270</sub> as  $R_H=12.1$  nm whereas its radius of gyration can be calculated as  $R_g = 1.27R_H = 15.2$  nm if one assumes  $\Theta$  conditions.

The silica nanoparticles utilized are the commercially available Ludox LS ( $R\sim 7$  nm) purchased from Sigma-Aldrich in a water dispersion. The surface of the nanoparticles possess -OH groups, so they can interact favorably with hydrophilic polymers such as PEO. From here on, the

nanoparticles will be denoted as NP<sub>7</sub>. The size of the nanoparticles was defined by Transmission Electron Microscopy and DLS measurements.

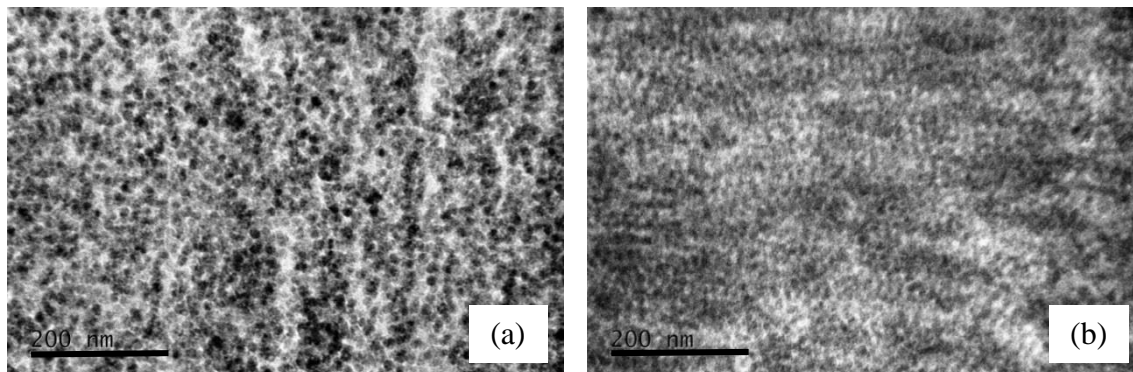


**Figure 1.** TEM images of PEO<sub>2270</sub> / NP<sub>7</sub> nanohybrids with (a)  $\phi_{\text{NP}} = 14\%$  and (b)  $\phi_{\text{NP}} = 53\%$  vol. The scale bar in both (a) and (b) is 200 nm.

The nanocomposites were prepared via solution mixing using the following procedure: The polymer was first diluted in water and left stirring for 24h. Then, the appropriate amount of nanoparticle dispersion was simply added to the solution. The samples were left to homogenize for 24h in a magnetic stirrer and, then, they were placed into Petri dishes and dried under vacuum. Before each measurement, the samples were left at 100°C for 15 min, in order to erase any thermal history, and, then, were cooled down to room temperature at a constant rate of 10°C/min, in order to ensure the same crystallizing conditions. The sample concentrations were measured as weight fraction utilizing Thermogravimetric Analysis and, then, volume fractions were calculated. The characteristics of the synthesized nanocomposites are reported in Table 1. In all nanohybrid compositions, the successful and homogeneous dispersion of the nanoparticles within the polymeric matrix was verified by Transmission Electron Microscopy as illustrated in Figure 1 for hybrids with 14 and 53 % vol NP<sub>7</sub> content.

**Table 1.** Details of the synthesized PEO<sub>2270</sub> / NP<sub>7</sub> and simulated PEO<sub>49</sub> / NP<sub>2</sub> nanocomposites

<b>Hybrids</b>	<b>w<sub>SiO<sub>2</sub></sub><sup>a</sup></b>	<b>φ<sub>SiO<sub>2</sub></sub><sup>b</sup></b>	<b><i>d</i><sup>c</sup></b>	<b><i>d</i>/R<sub>g</sub><sup>d</sup></b>
	<b>(wt)</b>	<b>(vol)</b>	<b>(nm)</b>	
PEO <sub>2270</sub> /NP <sub>7</sub>	0.25	0.14	2.156	0.142
PEO <sub>2270</sub> /NP <sub>7</sub>	0.70	0.53	0656-4.704	0.043-0.309
PEO <sub>2270</sub> /NP <sub>7</sub>	0.73	0.57	0.611-1.363	0.04-0.09
PEO <sub>2270</sub> /NP <sub>7</sub>	0.82	0.69	0.32	0.021
PEO <sub>49</sub> /NP <sub>2</sub>	0.05	0.02	11.58	6.81
PEO <sub>49</sub> /NP <sub>2</sub>	0.33	0.19	5.82	3.42
PEO <sub>49</sub> /NP <sub>2</sub>	0.57	0.39	4.59	2.70

<sup>a</sup> w<sub>SiO<sub>2</sub></sub>: weight fraction of the SiO<sub>2</sub> nanoparticles

<sup>b</sup> φ<sub>SiO<sub>2</sub></sub>: volume fraction of the SiO<sub>2</sub> nanoparticles

<sup>c</sup> *d*: the nearest inter-particle distance

<sup>d</sup> *d*/R<sub>g</sub>: the degree of chain confinement (R<sub>g</sub> is the radius of gyration of the bulk polymer chains)

Detailed atomistic molecular dynamics simulations of monodisperse poly(ethylene oxide) / silica, PEO/SiO<sub>2</sub>, nanocomposites were performed for nanohybrids of different concentrations of silica nanoparticles and at different temperatures. As reference, simulations of a bulk PEO with molecular weight MW=2,200 g/mol and methyl terminal groups at the same temperatures have been performed. The entanglement molecular weight of PEO chains is around 2000 g/mol<sup>99,100</sup>. Experimental systems consist of well-entangled PEO chains while in the model systems are mildly entangled. However, it is not expected entanglements to affect segmental dynamics. Following the notation of the material utilized experimentally, from here on, the simulated polymer is denoted as PEO<sub>49</sub> utilizing as subscript the number of its monomeric units. As nanoadditives, silica nanoparticles with almost spherical shape and radius of ~2.1 nm were utilized. All calculations were performed for three different concentrations of silica nanoparticles (i.e., 2% vol, 19% vol and 39% vol) and four different temperatures ranging from 330 up to 400 K. Details for all simulated systems are presented in Table 1 as well.

For the simulations, PEO<sub>49</sub> was represented by a united atom model and interactions were described by a modified united atom (UA) TraPPE based force field.<sup>93,101</sup> A full atom representation was used for the SiO<sub>2</sub> nanoparticle.<sup>102</sup> The particle-mesh Ewald (PME) method

was applied for the calculation of the electrostatic interactions. MD simulations were performed in the NPT statistical ensemble, where the pressure was kept constant with the use of Parrinello–Rahman barostat<sup>103</sup> and the temperature using the Nosé–Hoover thermostat.<sup>104</sup> The simulations were performed using the GROMACS simulation package.<sup>105</sup>

Typical snapshots of the model PEO<sub>49</sub>/ NP<sub>2</sub> systems are shown in Figure 2. A video from our MD simulation of hybrid polyethylene oxide/silica nanoparticle at 400 K is available at the Supporting Information.

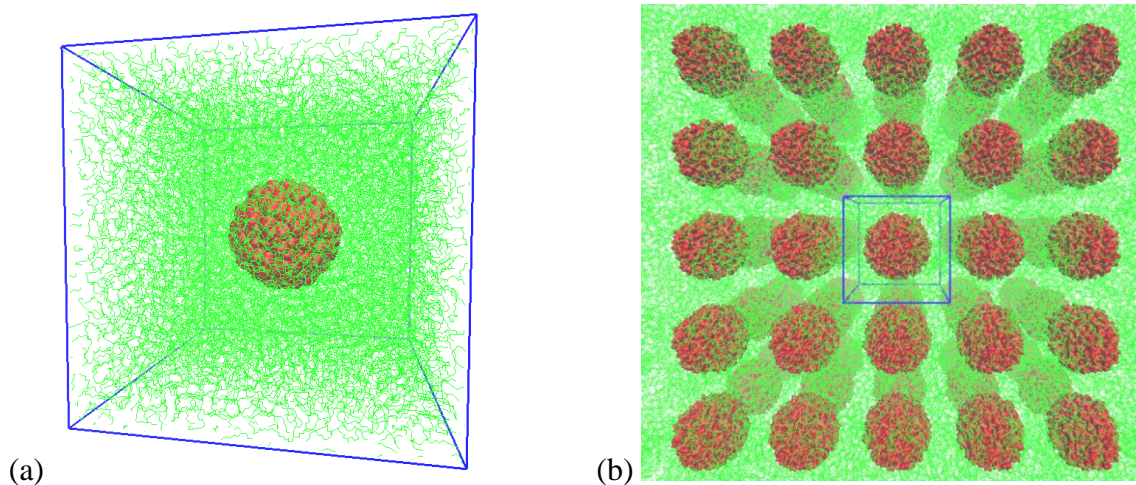


**Figure 2.** Snapshots of the model PEO/SiO<sub>2</sub> nanocomposite systems: (a) The PEO<sub>49</sub>/NP<sub>2</sub> hybrid system with a concentration of  $\phi_{\text{NP}} = 2\%$  at 400 K. (b) The PEO<sub>49</sub>/NP<sub>2</sub> hybrid system with the periodic images of the cubic simulation box that shows the simple cubic like structure of nanoparticles. The concentration is  $\phi_{\text{NP}} = 39\%$  and the temperature is 400 K. In both, the PEO<sub>49</sub> chains are shown green and the SiO<sub>2</sub> NP<sub>2</sub> red.

In general, the simulation protocol involves: (a) generation and equilibration of the PEO/SiO<sub>2</sub> model nanocomposites and (b) performing long atomistic MD simulations. Initial PEO/SiO<sub>2</sub> configurations were obtained from our previous work.<sup>13</sup> After generating the systems, equilibration MD runs for times up to 500 ns, depending on the system and the actual temperature, were performed, followed by long production runs, for times up to 1.0  $\mu\text{s}$ . During the simulations, a full relaxation, i.e., a complete decorrelation of the end-to-end vector, of the polymer chains is observed. For the calculated properties, analysis is performed over the last 0.8  $\mu\text{s}$  of the trajectory. It should be also noted that the simulation model systems consider a scenario of well-dispersed nanoparticles in a simple cubic arrangement induced by the periodic boundary

conditions, whereas experimental systems refer to rather random packing in the dispersion of the SiO<sub>2</sub> nanoparticles within the PEO matrix.

*b. Analysis Methods:*

The main goal is to study the spatial and dynamical heterogeneities of model hybrid polymer/nanoparticle systems in a detailed way at the molecular level. Consequently, the properties of the polymer chains are examined as a function of the distance from the SiO<sub>2</sub> nanoparticle center, by creating spherical shells of increasing radii (i.e., increasing distances from the SiO<sub>2</sub> center).

The mass density profiles were calculated in two ways. The first (radial type) is by using spherical shells of thickness equal to 1 Å, defined from the center-of-mass of the nanoparticles. Then, the polymer mass density is calculated within each shell. The second way of analysis involves a 3D reconstruction of the PEO mass density using a decomposition of the simulation box in rectangular parallelepipeds (cuboids) with dimensions of 3.2×3.2×4.46 Å. The choice of the cuboids dimension was a result of balance between the detail of the analysis and the statistical accuracy. The average mass of PEO atoms within each cuboid is calculated and divided with its volume.

The investigation of the dynamical properties of PEO chains involves the calculation of time correlation functions; for this reason, thicker, compared to the density, spherical shells are used. The choice of binning size (thickness of spherical shells) for the computation of each specific property is usually defined from the first minimum of density profile data, which defines the first adsorption layer.<sup>13,33,34</sup> In this work, for the calculation of the orientation autocorrelation function, three different analysis regimes were defined: (a) the whole simulation box, denoted as “Total”, (b) the adsorption region, i.e., 0-25 Å from the center of the nanoparticle (4-5 Å from the outer surface of the nanoparticle), denoted as “Ads”, defined based on the first minimum in the density profile, shown below, and (c) the whole simulation box except the adsorption region, denoted as “Matrix”. Note that for these calculations, the position of each segment/vector was monitored depending on the corresponding analysis regime, where it was initially located.

For the calculation of the desorption kinetics, the atoms that belong to the adsorption region at a given time  $t_0$  were first labeled. Then, for each time step  $t$ , these atoms were monitored and a function  $S(t + t_0)$  was defined that equals 1 when the atom is still within the adsorbed region and 0 when it is outside, i.e., when it is desorbed. Finally, the autocorrelation function of the adsorption state  $S$  was calculated as <sup>106</sup>:  $C_{\text{ads}} = \langle S(t + t_0) \bullet S(t_0) \rangle$ , where  $S(t_0) = 1$ . It is noted, that a buffer zone of 3Å (about the size of an atom) around the adsorption region shell was used, in order to take into account the fluctuations of the atoms that are located on the borders of the adsorption region. Therefore, an initially adsorbed atom is considered “desorbed” if it moves further than 28Å from the center (~8Å from the outer surface) of the nanoparticle. Last, during the analysis of all dynamical properties, and in order to improve statistics, the multiple time origin technique was used.

c. *Dielectric Relaxation Spectroscopy:*

Dielectric spectroscopy measures the complex dielectric permittivity  $\varepsilon^*(\omega)$  of a material as a function of angular frequency  $\omega$ . A homogeneous electric field, oscillating at frequency  $\omega$ , is applied to the sample, which is placed within the gap of a parallel plate capacitor. The molecular electric dipoles in the sample tend to be oriented by the field and, therefore, to rotate according to their molecular mobility at the given frequency and temperature <sup>107</sup>. The complex dielectric permittivity:

$$\varepsilon^*(\omega) = \varepsilon'(\omega) - i\varepsilon''(\omega) \quad (1)$$

provides the storage (real part,  $\varepsilon'$ ) and the loss (imaginary part,  $\varepsilon''$ ) dielectric contribution. A relaxation process is typically characterized by a peak in the spectrum of dielectric loss vs. frequency, centered at the relaxation frequency  $f_{\text{max}}=1/(2\pi \tau_{\text{max}})$ , where  $\tau_{\text{max}}$  is the most probable relaxation time of the process. The temperature dependence of the spectral features, like relaxation time, dielectric strength and peak width, provides information on the molecular dynamics of polar moieties, as the ones often found in polymer main chains or side groups, which can be influenced by both intra-and inter-molecular interactions as well as the properties and the interactions with the environment of the chain.

The dynamic measurements were performed utilizing a dielectric spectrometer (Alpha Analyzer, Novocontrol GmbH), in the frequency range  $10^{-2} - 10^7$  Hz. A thin film of the material under study was placed in a stainless steel parallel plate capacitor. The film was prepared by

uniaxially pressing each sample to form disks 12mm in diameter and 0.3-0.6mm in thickness. The pellets were annealed at 100°C in vacuum for 12 hours and adhered between indium foils to improve the electrical contact with the electrodes. The temperature was controlled through a heated flow of nitrogen gas, by Quatro Cryosystem (Novocontrol GmbH) in the range of 123 – 273 K. Measurements were performed isothermally in a pure nitrogen atmosphere. All samples were kept at 373 K for 30min and then cooled at 123 K with a rate of 10 K/min before the measurements whereas they were kept under nitrogen atmosphere throughout the measurements. During the measurements, the samples were constantly immersed in an inert nitrogen atmosphere.

When multiple relaxation processes are present, the analysis of the measured dielectric spectra is performed utilizing a superposition of empirical Havriliak-Negami functions, HN, together with an additional ionic conductivity contribution at low-frequencies and high temperatures. The functional form of the fitting function is:

$$\varepsilon^*(\omega) = \varepsilon_{\infty} + \sum_k \left[ \frac{\Delta\varepsilon_k}{\{1+(i\omega\tau_{HN,k})^{\alpha_k}\}^{\beta_k}} \right] + i \frac{\sigma_{dc}}{\varepsilon_0\omega} \quad (2)$$

where k is the index of the particular process,  $\tau_{HN,k}$  its Havriliak-Negami relaxation time,  $\Delta\varepsilon_k$  its dielectric (or relaxation) strength,  $\varepsilon_0$  the dielectric constant of the vacuum,  $\varepsilon_{\infty}$  the dielectric constant at frequencies much higher than the relaxation frequencies of all considered processes, and  $\alpha_k, \beta_k$  ( $0 < \alpha_k, \alpha_k\beta_k \leq 1$ ) are exponents describing the symmetric and asymmetric broadening of the distribution of relaxation times. It is noted that the Havriliak-Negami time,  $\tau_{HN}$ , and the position of the maximal loss,  $\omega_{max}$  are related via the expression  $\omega_{max} = \frac{1}{\tau_{HN}} \left[ \sin \frac{\alpha\pi}{2+2\beta} \right]^{1/\alpha} \left[ \sin \frac{\alpha\beta\pi}{2+2\beta} \right]^{-1/\alpha}$ <sup>107</sup>.  $\sigma_{dc}$  is the static dc conductivity determined by the fitting of the dielectric spectra by means of Eq. (2) or, equivalently, by the low frequency limit of the real part of the measured ac conductivity,  $\sigma'(\omega)$ .

### 3. Results and Discussion

#### 3.1 Static Properties:

The analysis of the model nanocomposite systems begins by probing directly the density heterogeneities at the PEO/silica interface. For this, the mass monomer density profile of the PEO<sub>49</sub> chains is calculated as a function of the distance from the center of mass of the SiO<sub>2</sub>

nanoparticle,  $r$ , as described in the previous section. Average density profiles, based on the center of mass of the monomers,  $\rho(r)$ , are presented in Figure 3a for all systems with concentration 2%, 19% and 39% vol at 400 K. The bulk density of PEO<sub>49</sub> at 400 K is also included (dashed horizontal line). A rather similar peak at a radial distance  $\sim 2.3$  nm (about 3-4 Å from the outer surface of the silica nanoparticles) is observed for all three systems denoting the attraction of the PEO<sub>49</sub> chains onto the NP<sub>2</sub>. As the distance from the surface of the nanoparticle increases, peaks of lower intensity follow up at 2.8 nm for 2% and 19% vol and at 3.2 nm for the 2% vol in NP<sub>2</sub> systems. It is noted that at longer distances, the bulk region is attained only for the 2% vol. In the systems with higher concentration in nanoparticles (more confined systems), the radial density profile of PEO<sub>49</sub> does not attain the bulk density. Moreover, in the case of the PEO<sub>49</sub> / NP<sub>2</sub> with 39% vol nanoparticle concentration, even the first peak of the density profile is roughly reached.

The monomer density profiles are presented in Figure 3b for various temperatures for the system with 19% vol concentration. A gradual decrease of the density is observed with increasing temperature, whereas the density curves retain the same characteristics. Similar temperature dependence is observed for the other two concentrations as well (data not shown here).

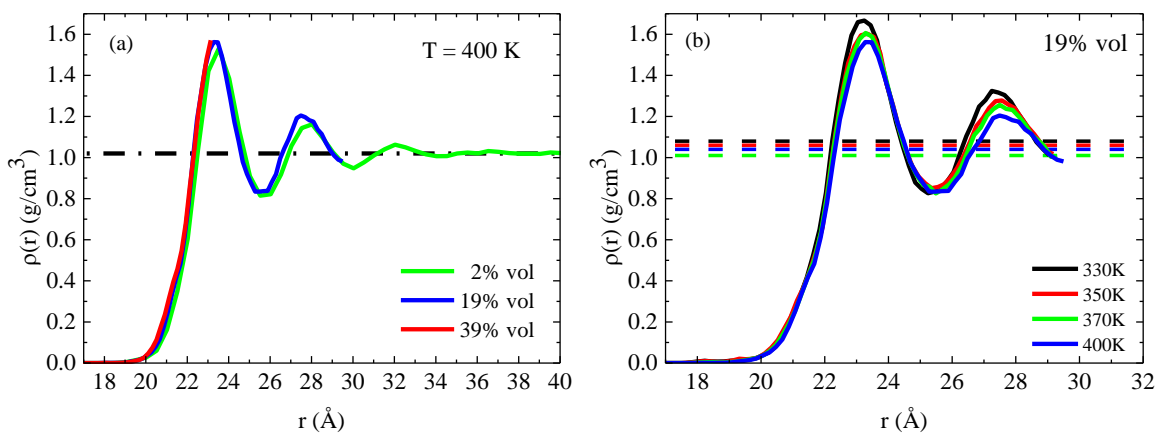


**Figure 3.** Mass monomer density profiles of PEO chains as a function of the distance from the SiO<sub>2</sub> nanoparticle center,  $r$ , for nanohybrids with: (a)  $\phi_{\text{NP}} = 2\%$ ,  $\phi_{\text{NP}} = 19\%$  and  $\phi_{\text{NP}} = 39\%$  in NP<sub>2</sub> at 400 K and (b)  $\phi_{\text{NP}} = 19\%$  NP<sub>2</sub> concentration at 330, 350, 370 and 400 K. The dashed lines correspond to the bulk PEO<sub>49</sub> values at each temperature.

The above analysis, using spherical shells, neglects parts of the (cubic) simulation domain, mainly the parts that are situated at its corners. Therefore, a more complete picture of the polymer density is provided through the calculation of the density profile in three dimensions, using a “3D polymer density tomography” as described in the Analysis Methods Section. Based on the analysis described there, the 3D density profile is calculated throughout the simulation box, scanning its volume and exploring various cross sections from the bottom to the top, as presented schematically in Figure 4f. Slices of increasing distance from the center of the SiO<sub>2</sub> nanoparticle, parallel to the *xy* plane, are presented in Figure 4a-4e accordingly. Slices have thickness of 3.2 Å and correspond to distances of 1.5 Å (slice A), 8.4 Å (slice B), 15.3 Å (slice C), 22.2 Å (slice D) and 29.1 Å (slice E) from the central plane.

In Figure 4, the density of PEO<sub>49</sub> is shown with different colors. Blue is the region of the nanoparticle (zero density of PEO), whereas yellow corresponds to regions with density very similar to the (average) bulk value whereas red denotes regions with density higher than that of the bulk polymer. It is clear from all the data referring to regions (slices) around the nanoparticle that shell-like areas (“rings”) of different PEO density are observed. For the closest spherical shell to the nanoparticle (cyan region) the roughness of its surface, allows some polymer amount to be attached on it, but PEO density is smaller than the bulk PEO value. The next (red) ring corresponds to the first adsorption shell (i.e., the first peak of the radial density profile shown in Figure 3), whereas consequent rings indicate a gradual decrease of PEO density towards its bulk value, with moving away from the NP. However, it is interesting to observe that for all slices the polymer density attains values similar to the bulk one on the face diagonal of the simulation box. Therefore, it is clear that even for the most confined system investigated computationally, a considerable amount of polymeric material exists at the corners of the simulation domain, where the effect of the nanoparticle on its properties is attenuated. This is not obvious in the radial density profiles, since the analysis in radial distances from the center of the NP (spherical shells) does not allow to cover these (corner) regions. A video of the 3D representation of the PEO<sub>49</sub> density profiles in the PEO/SiO<sub>2</sub> system is available at the Supporting Information.

Furthermore, we analyzed the bridge conformations of the PEO chains, i.e. sequence of atoms of the same PEO chain connecting adsorbed atoms in different SiO<sub>2</sub> nanoparticles. From our analysis we found that the bridging percentage between two nanoparticles is about 70-80% for the systems with concentration of  $\phi_{\text{SiO}_2} = 39\%$  and 22-25% for the systems with  $\phi_{\text{SiO}_2} = 19\%$ . For

the systems with concentration of  $\varphi_{\text{SiO}_2} = 2\%$  there is no bridging. There was no found strong dependencies with temperature; the above percentages are very similar, within error bars, for all temperatures studied here. Those percentages can be affecting the mechanical and/or the rheological properties of the hybrid material.

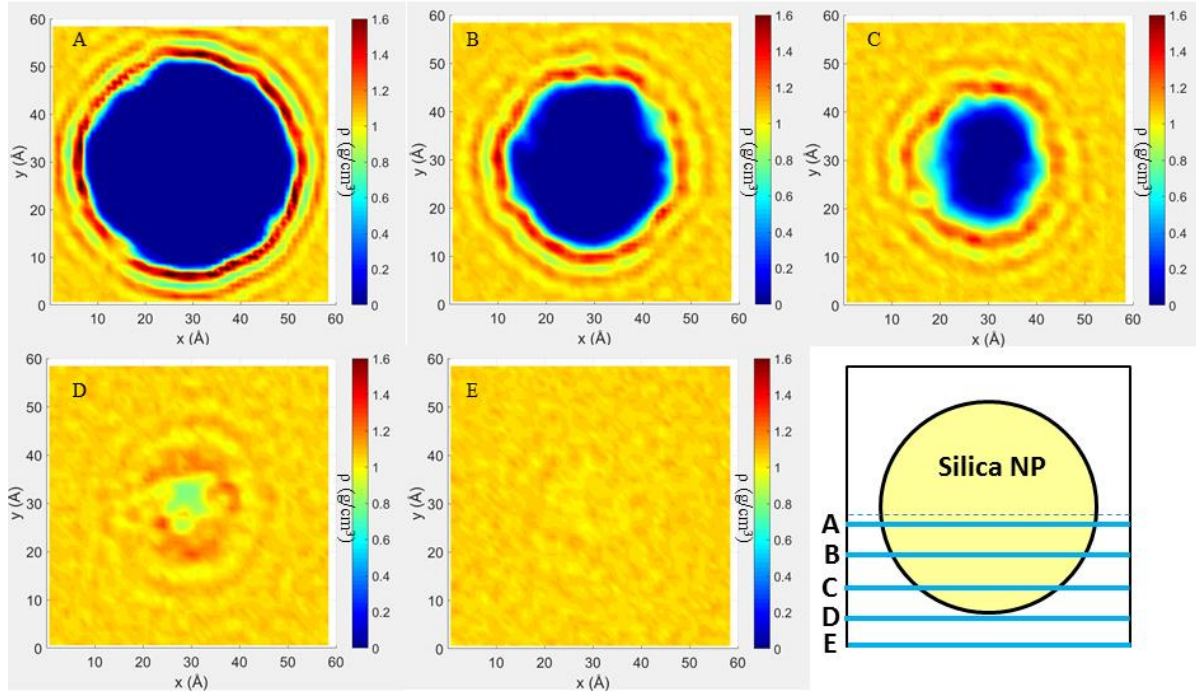


**Figure 4.** 3D representation of the PEO<sub>49</sub> density profiles in the PEO/SiO<sub>2</sub> system with  $\varphi_{\text{NP}} = 19\%$  at 400 K. Different slices, of 3.2 Å thickness, parallel to the  $xy$  plane are used at various distances from the center-of-mass of the NP<sub>2</sub>: 1.5 Å (slice A), 8.4 Å (slice B), 15.3 Å (slice C), 22.2 Å (slice D) and 29.1 Å (slice E). At the bottom right, a sketch of the polymer nanocomposite system illustrates the five slices. The distances scaled with the radius of the silica NP<sub>2</sub> are: 0.07 (slice A), 0.40 (slice B), 0.73 (slice C), 1.06 (slice D) and 1.38 (slice E).

### 3.2 Dynamical properties of PEO chains in the model PEO/SiO<sub>2</sub> systems

#### 3.2.1 Orientational dynamics at the monomeric level

The dynamic properties of the PEO/SiO<sub>2</sub> nanocomposites, especially with increasing the spatial confinement of the chains have been investigated utilizing a combined experimental and theoretical approach. The orientational dynamics is studied at the segmental level using the time

autocorrelation function (ACF) of the second Legendre polynomial, for the  $v_{1-3}$  vector, which connects two non-consecutive atoms, defined as:

$$P_2(t) = \frac{3}{2} \langle \cos^2 \theta(t) \rangle - \frac{1}{2} \quad (3)$$

where  $\theta(t)$  is the angle of this vector at time  $t$  relative to its position at  $t = 0$  and the brackets denote ensemble average.

Autocorrelation functions of  $P_2(t)$  are presented in Figure 5 and Figure 6 for all hybrid PEO/SiO<sub>2</sub> nanocomposites studied in the current work together with the corresponding data for the respective bulk PEO system. Figure 5 presents  $P_2(t)$  as a function of time for all three volume fractions of 2%, 19% and 39% vol at 400 K. Calculations have been performed in two shells with respect to the surface of the nanoparticle 0-25 Å (i.e., the adsorption region “Ads”) and 25-end Å (i.e., the rest area “Matrix”) as well as on the entire box, probing the average value (“Total”). In all cases, slower decorrelation is observed in the first adsorption shell, whereas the average curve lies between the “Ads” and “Matrix” area. The effect of confinement (i.e., of different concentrations) becomes clear comparing the three figures: starting from the nanocomposite with the smaller concentration of 2% vol in nanoparticles (less confined polymer chains), the three curves corresponding to the bulk PEO, the “Matrix” and the “Total” almost coincide, indicating the predominance of the bulk behavior in this concentration. As the amount of the nanoparticles increases, the ratio of the chains in the “Matrix” vs the “Ads” chains decreases. In a moderate confinement (19% vol), the “Matrix” still prevails (like for the low concentration) defining the total dynamics in this case as well, however with slower relaxation times; differences between the curves of the hybrid system and the corresponding bulk curve can be observed. On the contrary, for the most confined system (39% vol), there is an obvious difference in the autocorrelation curves between the “Ads” and the “Matrix” as well as between all curves of the hybrid system and the corresponding bulk curve with the latter being much faster.

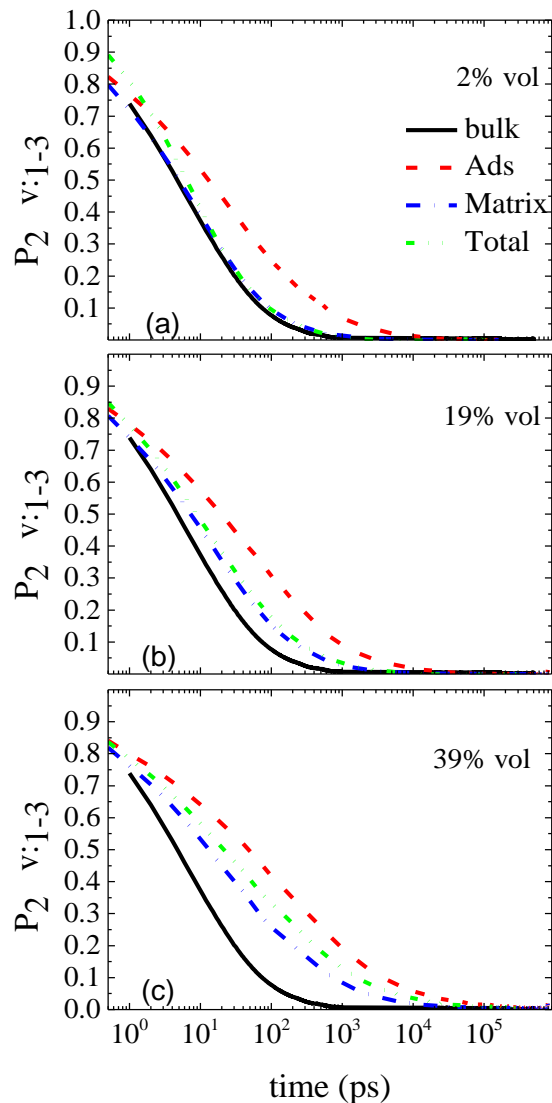


**Figure 5.** Time autocorrelation function of the vector connecting two non-consecutive atoms along a monomer,  $P_2(t)$ , as a function of time for the characteristic vector  $v_{1-3}$  of poly(ethylene oxide) for all systems at 400 K. (a)  $\phi_{\text{NP}} = 2\%$ ; (b)  $\phi_{\text{NP}} = 19\%$ ; (c)  $\phi_{\text{NP}} = 39\%$ . In all cases, the corresponding curve for the bulk polymer is shown as well.

Differences among the systems of different concentrations become clearer in Figure 6a and Figure 6b, where a direct comparison of the relaxation of the autocorrelation function in each shell distinctly is provided at 400 K. It is clear, that for the first adsorbed layer, there is a significant deviation from the bulk dynamics, which becomes more and more significant with increasing the nanoparticle content, with the bulk dynamics being the fastest. The dynamics of

the “Matrix” slows down with respect to the bulk with increasing the nanoparticle content as well, however less strongly than the respective one in the adsorbed layer.

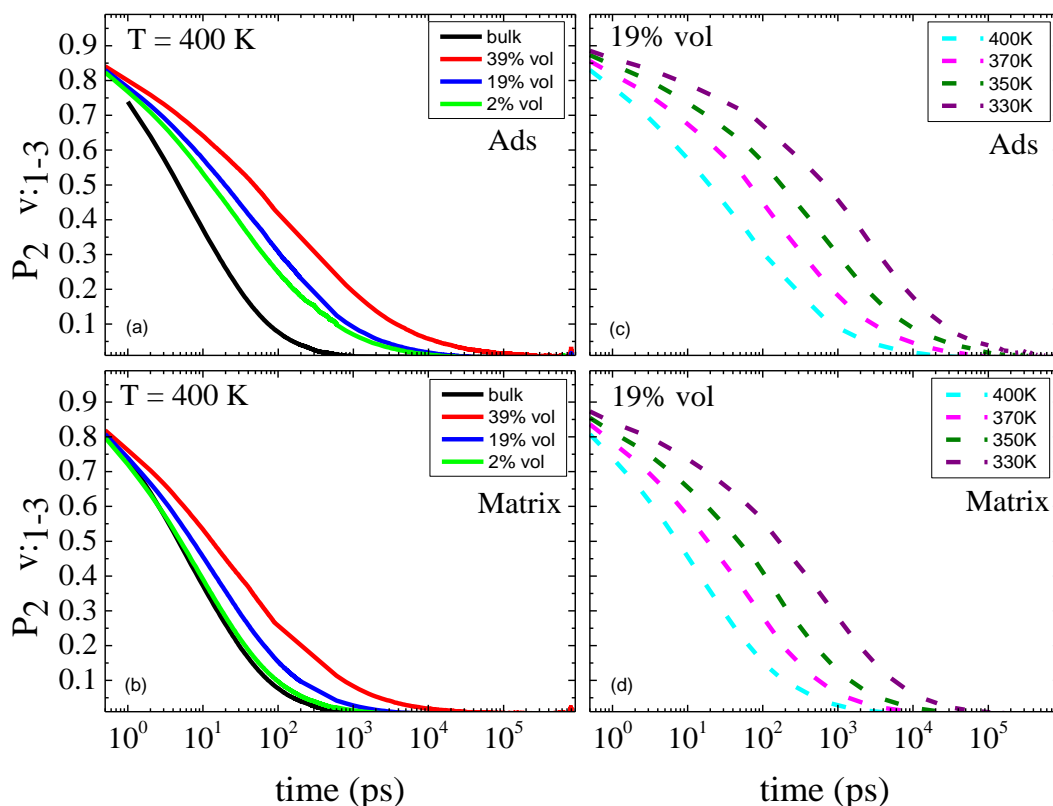


**Figure 6.** Autocorrelation function of bond order parameter  $P_2(t)$  as a function of time for the characteristic vector  $v_{1-3}$  of poly(ethylene oxide) for (a) all concentrations in the “Ads” shell at  $T=400$  K; (b) all concentrations in the “Matrix” at  $T=400$  K; (c) all simulated temperatures in the “Ads” shell of the  $\phi_{NP} = 19\%$  nanocomposite; (d)  $P_2(t)$  all simulated temperatures in the “Matrix” of the  $\phi_{NP} = 19\%$  nanocomposite. In (a) and (b) the corresponding curves for the bulk polymer is shown as well.

In Figure 6c and Figure 6d the temperature dependence of the autocorrelation relaxation function  $P_2(t)$  is depicted. The curves are presented at four different temperatures for the segments in the “Ads” and “Matrix” areas. As expected, the decorrelation is faster at higher temperatures with a gradual retardation from 400 K to 330 K; however, it is clear that all dynamics is slower in the “Ads” than in the “Matrix” area for all temperatures. The above observations can be quantified by analyzing the autocorrelation functions and the determination of the corresponding segmental relaxation times. The autocorrelation functions were analyzed

using a pair of Kohlrausch-Williams-Watts (KWW) stretch exponential functions to effectively fit the curves and the segmental times were derived by integrating the fit curve as the most probable relaxation time. This procedure was followed since utilization of a single KWW failed to fit the data successfully. Segmental relaxation times of PEO chains for all systems are presented as a function of inverse temperature in Figure 7. The values for the polymer in the bulk are also included for comparison.

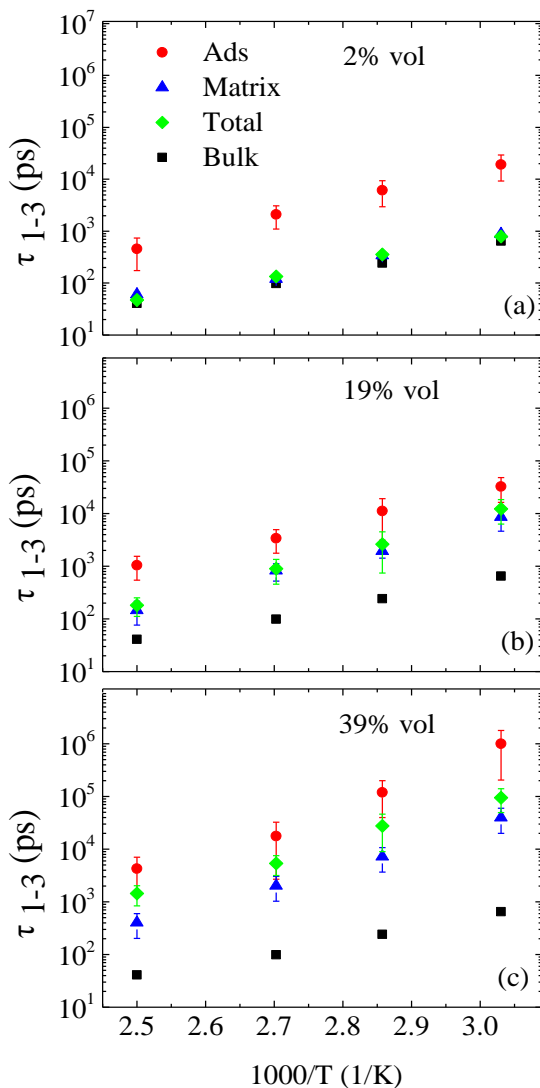


**Figure 7.** Segmental relaxation time,  $\tau_{\text{seg}}$ , of  $v_{1-3}$  characteristic vector determined by analyzing the  $P_2(t)$  time autocorrelation functions for all simulated systems: (a)  $\phi_{\text{NP}} = 2\%$ ; (b)  $\phi_{\text{NP}} = 19\%$ ; (c)  $\phi_{\text{NP}} = 39\%$ .  $\tau_{\text{seg}}$  for “Ads” and “Matrix” chains are shown, as well as the average values for the entire systems (“Total”) and the values for PEO<sub>49</sub> in the bulk.

As expected, the segment relaxation time  $\tau_{\text{seg}}$  increases as temperature decreases, for all model PEO<sub>49</sub>/NP<sub>2</sub> systems. Starting from the nanocomposite with the smallest volume fraction of nanoparticles (2% vol, Figure 7a), it is clear that the dynamics of polymer segments at the vicinity of the PEO/SiO<sub>2</sub> interface (“Ads” region) is slower than the ones in the “Matrix” region; for all temperatures  $\tau_{\text{seg}}$  of “Ads” segments is about 10 times larger than the “Matrix” ones. On the contrary, the dynamics of the segments in the “Matrix” region is very similar to the bulk one (black squares). The average dynamics in the nanocomposite (“Total” data) is also very similar to the bulk, since the percentage of “Ads” segments over their total number is calculated to be only about 2%; therefore, it is very small to affect the overall dynamic behavior.

As the concentration of the nanoparticles increases, the effect of the confinement on the segmental dynamics of PEO becomes more important. The data for the system with 19% volume fraction of nanoparticles, shown in Figure 7b, indicate that the “Ads” segments exhibit relaxation times about  $\sim 10$  times larger than the “Matrix”, which are  $\sim 10$  times slower than the corresponding values in the bulk as well. The percentage of “Ads” segments is about 18%, so the average dynamics (“Total” data) are again very close to the ones for the “Matrix” region.

Even stronger is the effect of confinement on the segmental dynamics of the PEO chains for the model PEO<sub>49</sub>/NP<sub>2</sub> systems with the highest concentration of nanoparticles studied computationally (39% vol, Figure 7c). Similarly to the systems with concentration 19% vol, the “Ads” segments exhibit relaxation times about  $\sim 10$  times larger than the “Matrix”; however, now the latter are about 100 times larger than the ones in the bulk. In addition, the values for the average dynamics (“Total”) is in between the values for the “Ads” and “Matrix” regions; this is not surprising if one considers the large fraction of “Ads” segments for these systems (about 44%) compared to the ones with lower nanoparticle concentrations. Finally, for the strongly confined PEO chains, the corresponding differences in  $\tau_{\text{seg}}$  are more pronounced for systems at low temperatures; for example, at T=330 K the ratio between the “Ads” and the “Matrix” segments is  $\sim 25$  times whereas the ratio between the “Matrix” and the bulk is  $\sim 60$  times.

### 3.2.3 Desorption kinetics

In order to better understand and interpret the findings on the computationally derived PEO segmental dynamics in the PEO<sub>49</sub> / NP<sub>2</sub> nanocomposites, the desorption times of the polymer

segments from the surface of the nanoparticle were calculated. Figure S1 shows the autocorrelation functions  $C_{\text{ads}}$  of the adsorption state S (see Section 2) of the polymer atoms for all examined temperatures and concentrations. Polymer atoms desorb from the vicinity of the PEO/SiO<sub>2</sub> interface (adsorption shell) faster at higher temperatures, as expected, for all concentrations. The desorption times of all systems are presented in Figure 8, calculated as the integral of the curves presented in Figure S1. As a result of the strong confinement, there is an obvious retardation of PEO atoms to desorb from the surface of the nanoparticle at all temperatures in the system with 39% vol NP<sub>2</sub>. It is noted that differences in the desorption times are larger between the nanohybrids with 39% vol and 19% vol nanoparticles when compared to those between the 19% vol and 2% vol NP<sub>2</sub>. Analogous trends were observed to the corresponding decorrelations of the  $P_2(t)$  for the  $v_{1-3}$  characteristic vector (Figure 5-Figure 7).

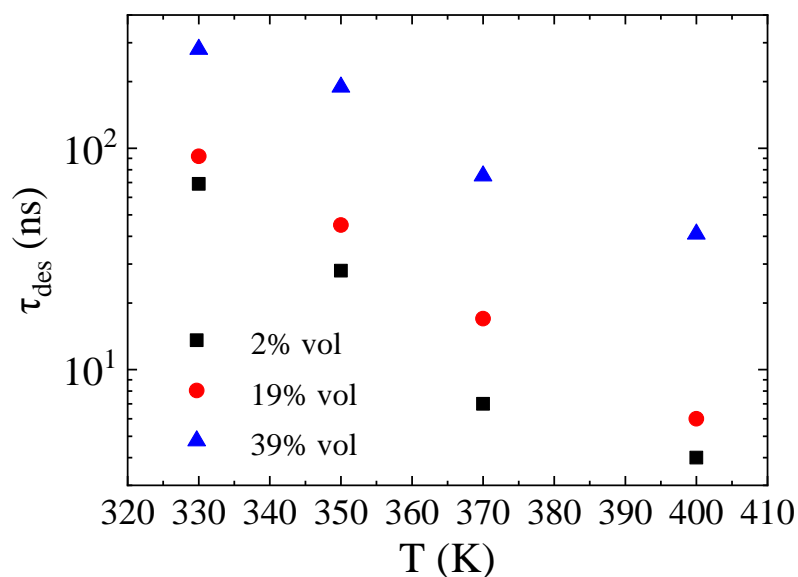


**Figure 8.** Desorption times of the polymer chains,  $\tau_{\text{des}}$ , being in the first adsorption shell 0-25 Å from the center of the nanoparticle for all simulated nanohybrids. The error bars are about 5-15% of the actual values.

### 3.3 Segmental dynamics of PEO chains in PEO/SiO<sub>2</sub> via dielectric spectroscopy

The dynamic properties of the high molecular weight PEO<sub>2270</sub> / NP<sub>7</sub> nanocomposites, in the dynamic range of the segmental relaxation were investigated experimentally by Dielectric Relaxation Spectroscopy.

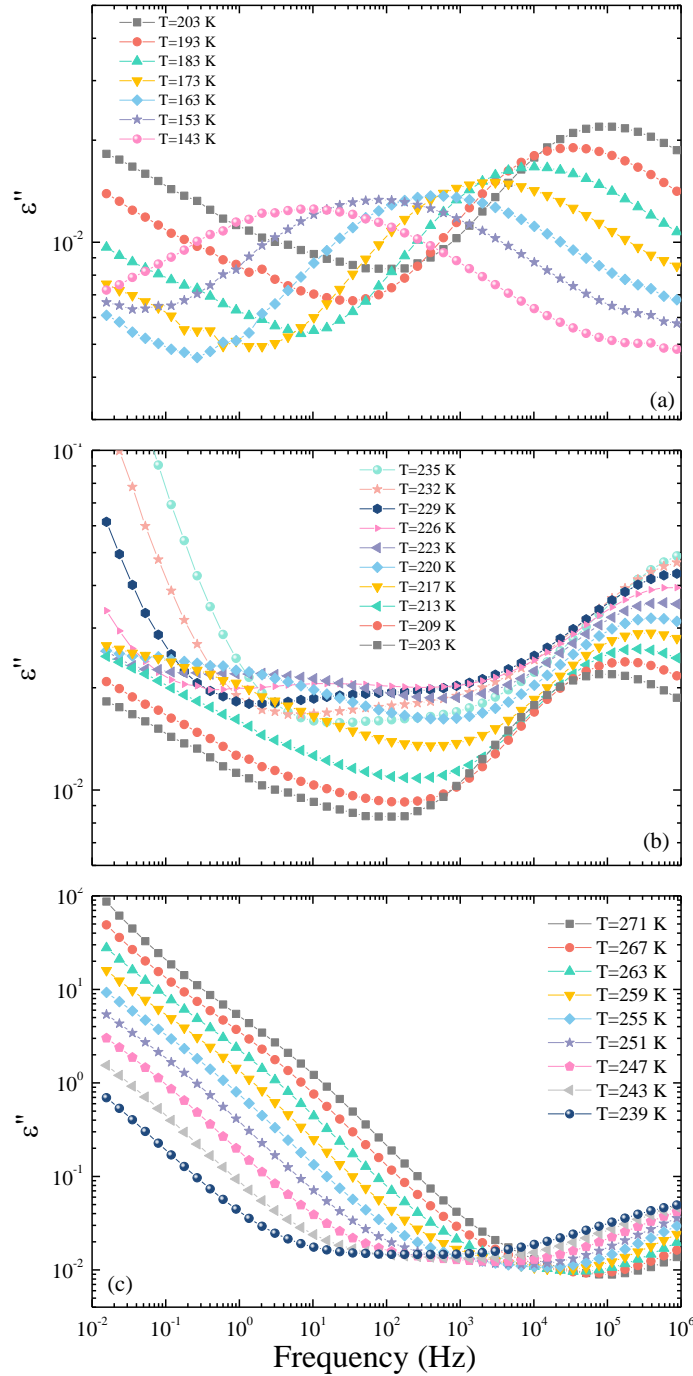


**Figure 9.** Temperature dependence of the imaginary part,  $\epsilon''$ , of the complex permittivity for the bulk PEO<sub>2270</sub> in the (a) low, (b) intermediate and (c) high temperature regime.

Figure 9 shows the frequency dependence of the imaginary part of the complex permittivity in the low (Figure 9a), intermediate (Figure 9b) and high (Figure 9c) temperature regime, for the bulk PEO<sub>2270</sub>. A very broad peak, covering almost six-seven orders of magnitude in frequency, is observed at low temperatures, below the glass transition temperature,  $T_g$ , that shifts towards higher frequencies as temperature increases. This sub- $T_g$  relaxation process, can be attributed to the motion of hydroxyl groups, and other local motions, the so called  $\beta$ -process according to the literature<sup>27,107</sup>. Above  $T_g \sim 206$  K, the  $\beta$ -process moves out of the frequency window and another process, which is the segmental relaxation, emerges. Both  $\alpha$ - and  $\beta$ -relaxation processes are very broad, with the  $\beta$ -process exhibiting higher relaxation strength. In the higher temperature range, the  $\alpha$ - process is observed together with the Maxwell-Wagner relaxation process, which is a process caused by the spatial inhomogeneity of dc conductivity profile, for example in the interfaces between the polymer and the silica.

Dielectric relaxation spectroscopy measurements were performed for PEO<sub>2270</sub>/NP<sub>7</sub> nanocomposites with different compositions in nanoparticles. Figure 10 shows the frequency dependence of the imaginary part of the complex permittivity for the four PEO<sub>2270</sub>NP<sub>7</sub> nanocomposites measured for temperatures both below and above the glass transition temperature of the bulk PEO<sub>2270</sub>. In all cases, the measured spectra resemble the measurements of the neat polymer. In the low temperature range the  $\beta$ -process dominates the spectrum for all hybrids, moving towards higher frequencies as temperature increases. In all cases, around 203 K, which is close to the glass transition temperature of the bulk polymer, the  $\alpha$ -process enters the frequency window. For the nanohybrid with the highest content of NP<sub>7</sub>, i.e., with 69% vol, the peak of the  $\alpha$ -process interferes with that of the Maxwell-Wagner process, the contribution of which becomes more significant as the concentration of nanoparticles increases resulting in a higher fraction of the overall interfaces present in the nanohybrid material.

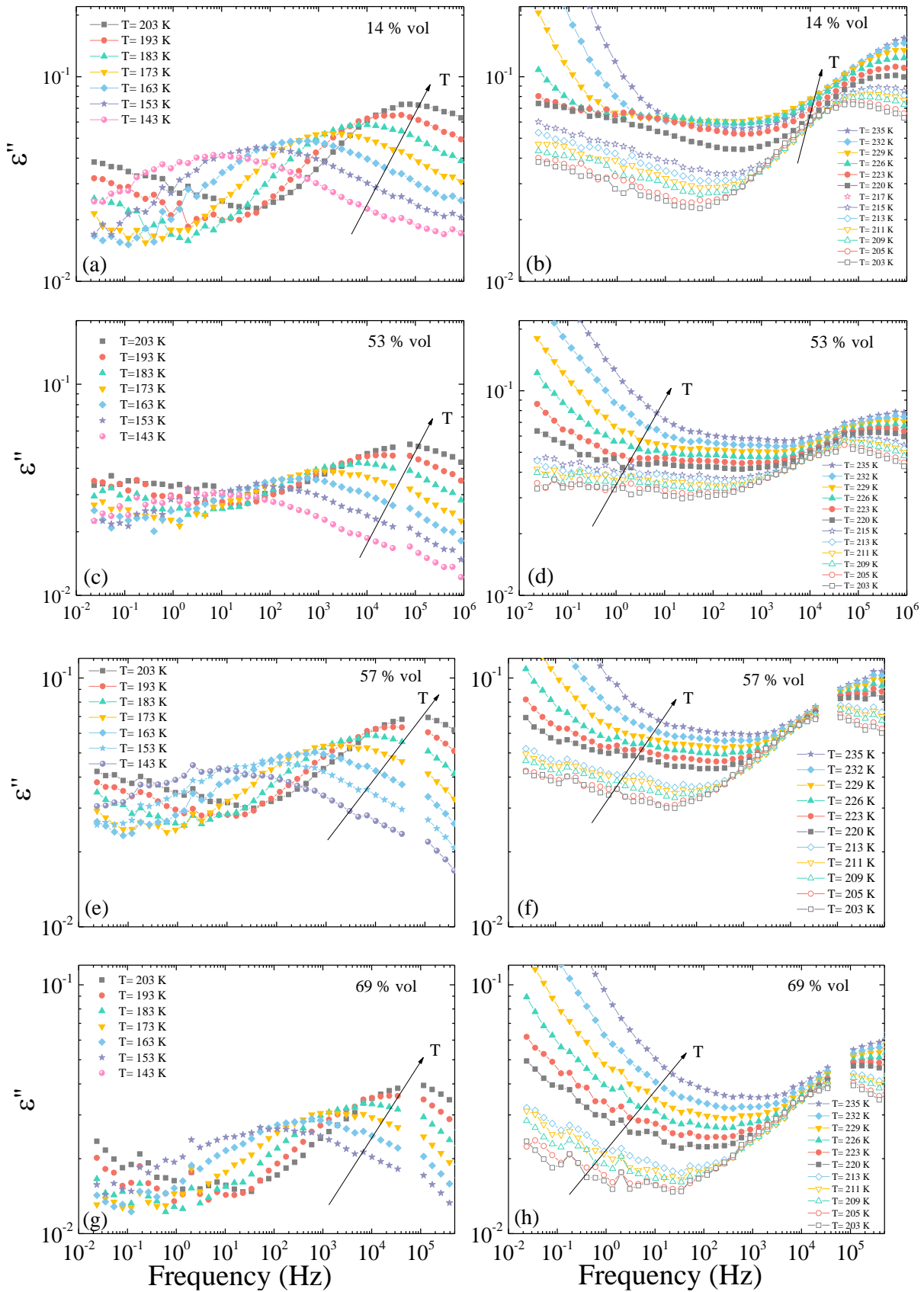


**Figure 10.** Frequency dependence of the imaginary part of the dielectric relaxation of the PEO<sub>2270</sub> / NP<sub>7</sub> nanohybrids with (a,b)  $\phi_{\text{NP}} = 14\%$ , (c,d)  $\phi_{\text{NP}} = 53\%$ , (e,f)  $\phi_{\text{NP}} = 57\%$  and (g,h)  $\phi_{\text{NP}} = 69\%$  at temperatures below (a,c,e,g) and above (b,d,f,h) the glass transition temperature of the bulk PEO<sub>2270</sub>.

For the quantitative comparison of the dielectric relaxation measurements and in order to identify the different relaxation processes and determine the relation between the relaxation times of the polymer in bulk and under confinement in the nanohybrids, the dielectric data were analyzed utilizing a linear superposition of empirical Havriliak–Negami (HN) functions (Eq. 2). An additional ionic conductivity contribution is added to the fitting formula at low-frequencies and high temperatures accounted for by an  $\omega^{-1}$  dependence. A representative analysis of the spectra for three temperatures, below, around and above the glass transition temperature of the neat polymer,  $T_g$ , for the neat PEO<sub>2270</sub> and for the nanohybrid with 57% vol NP<sub>7</sub> is shown in Figure 11. Multiple relaxation processes are necessary in all cases in order to obtain a good fit to the data. For the neat polymer (Figure 11a), the shape and relaxation strength parameters for the fast process are determined from the spectra at low temperatures. Therefore, for the local  $\beta$ -process the  $\beta$  parameter is fixed at 0.55 whereas the  $\alpha$  (0.35-0.6) and  $\Delta\epsilon$  (0.3-0.6) parameters increase with increasing temperature. At higher temperatures (Figure 11b and Figure 11c), close and above  $T_g$ , the  $\alpha$ -process appears and its  $\beta$  parameter is fixed at 1.0, while its  $\alpha$  is determined around 0.2-0.45 and  $\Delta\epsilon$  is constantly decreasing from 0.2 to 0.05. At even higher temperatures (not shown) and at low frequencies, the addition of a contribution due to ionic conductivity is necessary as a line with a slope of  $\sim -1$ . A similar analysis was performed for the spectra of all nanohybrids (Figure 11d, Figure 11e and Figure 11f for PEO<sub>2270</sub>/NP<sub>7</sub> with 57% vol in NP<sub>7</sub>). The shape and relaxation strength parameters are determined at low temperatures for the fast processes as well, similarly to the case of both the bulk polymer whereas at higher temperatures, above the bulk  $T_g$ , the  $\beta$  parameter of the  $\alpha$ -process was fixed at 1.0. All parameters of the Havriliak-Negami functions used in the fits for all the processes of all the hybrids as well as those of pure PEO<sub>2270</sub> are reported in Table 2.

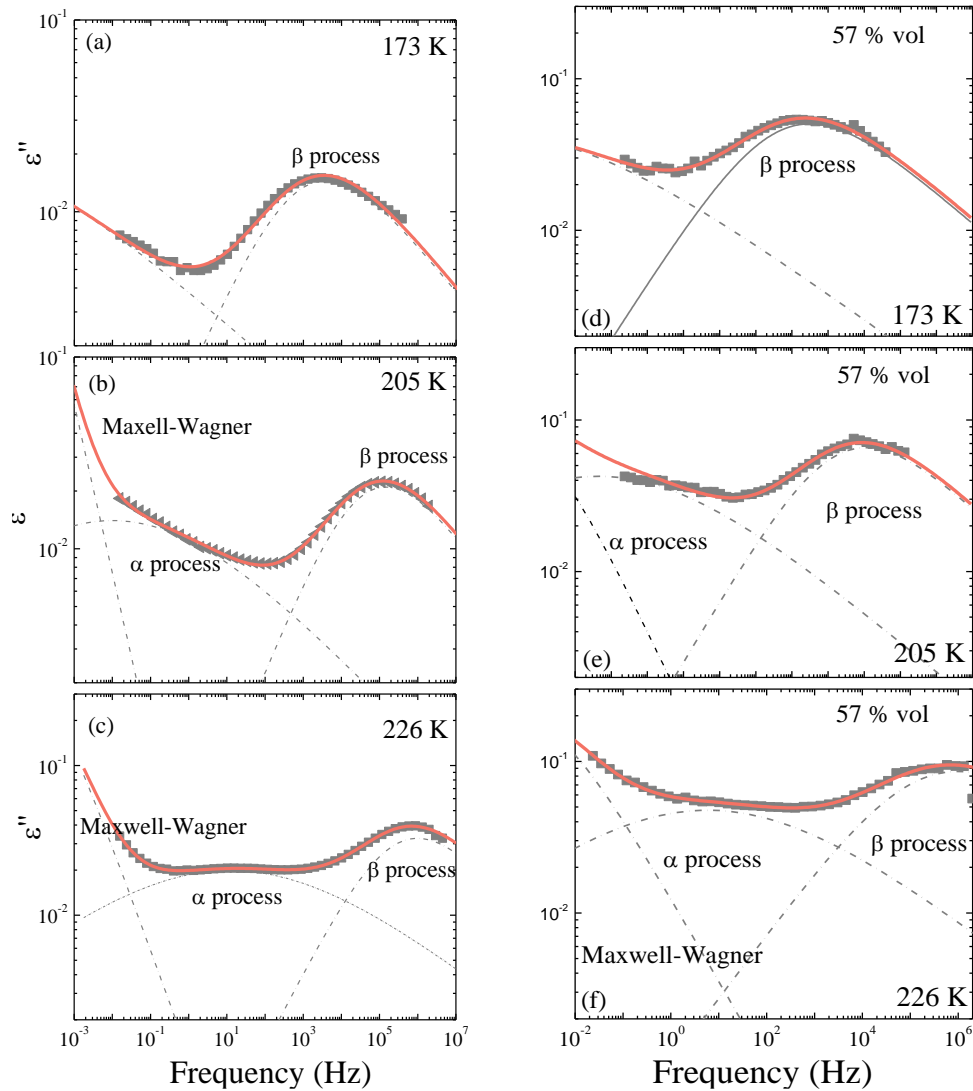


**Figure 11.** Imaginary part of the dielectric permittivity,  $\epsilon''$ , for (a, b, c) the pure PEO<sub>2270</sub> and (d, e, f) for PEO<sub>2270</sub>/NP<sub>7</sub> at (a, d)  $T = 173$  K, well below the  $T_g$ , (b, e)  $T = 205$  K, around the  $T_g$ , and (c, f)  $T = 226$  K, above the  $T_g$ . The peaks that contribute to the individual relaxation processes ( $\beta$ ,  $\alpha$ , Maxwell-Wagner polarization) are shown with black lines, whereas the red lines are the total fits.

**Table 2.** Fitting parameters of the Havriliak-Negami functions for PEO<sub>2270</sub> and PEO<sub>2270</sub>/NP<sub>7</sub> nanocomposites

Sample	Process	$\alpha$	$\beta$	$\Delta\epsilon$
PEO <sub>2270</sub>	$\alpha$ -process	0.2-0.45	1	0.2-0.05
	$\beta$ -process	0.3-0.6	0.55	0.3-0.6
$\phi_{NP} = 14\%$	$\alpha$ -process	0.23-0.25	1	0.5-0.4
	$\beta$ -process	0.4-0.5	0.55	0.4-0.9
$\phi_{NP} = 53\%$	$\alpha$ -process	0.18-0.2	1	0.5-0.2
	$\beta$ -process	0.3-0.6	0.55	0.3-0.25
$\phi_{NP} = 57\%$	$\alpha$ -process	0.17-0.3	1	0.6-0.45
	$\beta$ -process	0.35-0.5	0.55	0.4-0.7
$\phi_{NP} = 69\%$	$\alpha$ -process	0.15-0.48	1	0.23-0.16
	$\beta$ -process	0.37-0.45	0.55	0.23-0.5

The relaxation times obtained by this analysis are shown in Figure 12, in an Arrhenius representation for the neat PEO<sub>2270</sub> and all PEO<sub>2270</sub>/NP<sub>7</sub> nanocomposites.

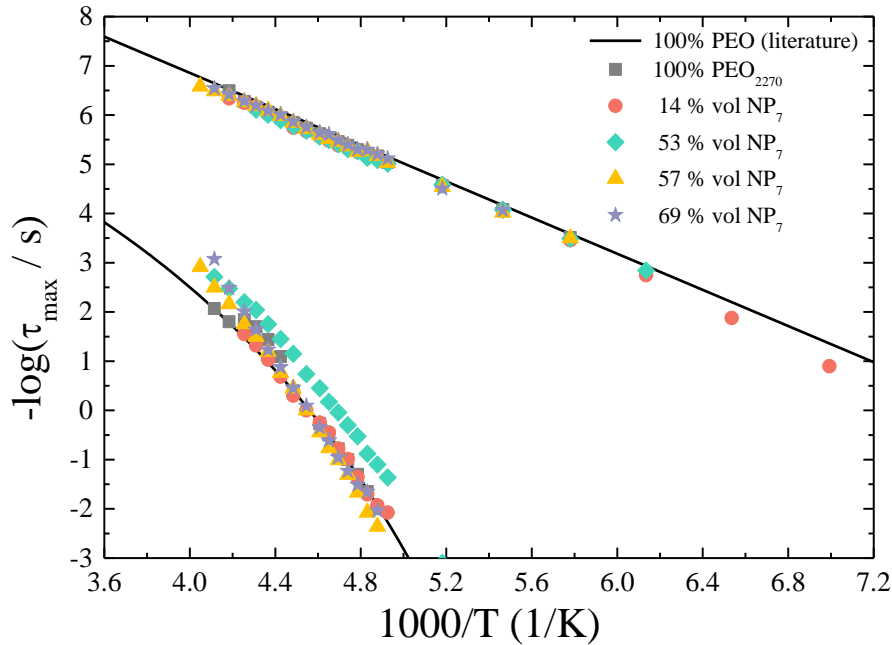


**Figure 12.** Arrhenius relaxation map for the neat PEO<sub>2270</sub> and the PEO<sub>2270</sub>/NP<sub>7</sub> nanocomposites. The lines are the results of an Arrhenius (for the  $\beta$ -relaxation) and of a VFT (for the  $\alpha$ -relaxation) fit obtained from the literature<sup>27</sup> for the same polymer.

The  $\beta$ -process for the neat PEO<sub>2270</sub> follows an Arrhenius temperature dependence  $\tau = \tau_{0,\beta} \exp[E/RT]$  with a single activation energy  $E=35$  kJ/mol and a  $\tau_{0,\beta} = 9 \cdot 10^{-15}$  s, which are characteristic of a local process and are in close agreement with the values reported for PEO in literature (showed with a black line)<sup>27</sup>. The nanocomposites show a very similar behavior with activation energies,  $E_{14} = 36.5$  kJ/mol,  $E_{53} = 34$  kJ/mol,  $E_{57} = 35$  kJ/mol and  $E_{69} = 35.4$  kJ/mol, respectively. It is noted that the similarity in the relaxation times and of their temperature dependence of the  $\beta$ -relaxation is anticipated, since this is a very local process that is not significantly affected by spatial confinement unless there are specific interaction in the systems like for example existence of a hydrogen bond network<sup>25,58,59</sup>. Around the glass transition  $T_g$  of the polymer, the segmental process emerges, as a result of the relaxation of cooperatively rearranging regions of a few repeat units. The temperature dependence of this process appears to follow the Vogel–Fulcher–Tammann (VFT) equation,  $\tau = \tau_{0,\alpha} \exp[A/(T - T_0)]$ , and is in very good agreement with the values found in literature shown as black line, as well<sup>27</sup>. The nanocomposites do not exhibit a very different dynamic behavior in comparison to that of the

bulk polymer and it seems that the confinement, which should be considered severe, especially for the nanohybrids with high nanoparticle content, does not influence the dynamics to any detectable degree. This behavior is considerably different than what was obtained experimentally for polymer nanocomposites composed of either poly(ethylene oxide) or different linear or hyperbranched polymers and layered inorganic nanoadditives. It is noted, that according to our previous study on PEO confined within the galleries of layered silicate, the sub- $T_g$  ( $\beta$ -process) was not affected by the confinement, while the segmental relaxation ( $\alpha$ -process) disappeared for hybrids containing only chains under confinement within the galleries of the inorganic montmorillonite, with a new process ( $\alpha'$ -process attributed to confined chains) appearing exhibiting an Arrhenius temperature dependence. In the current case the  $\alpha$ -process is always present in the nanohybrids and no new process appears. The  $\alpha$ -process of the nanohybrid with 14% vol NP<sub>7</sub> is identical to that of the pure polymer, while the segmental relaxation times of the other nanocomposites examined indicate a tendency towards a more Arrhenius temperature dependence, thus, the polymer behaves as a stronger glass, especially for the hybrids with high silica loadings. However, the differences of the nanocomposites compared to the pure polymer are very weak, indicating, again, that the confinement in this system is not as severe as in the case of the PEO-Na<sup>+</sup>-MMT system and/or that a large amount of bulk-like polymer exists in the nanohybrids due to the geometry of the nano-additives despite the high number of nanoparticles.

#### **4. Discussion and Conclusions**

In this work, PEO/SiO<sub>2</sub> nanocomposites have been studied via a combined simulation and experimental approach involving detailed atomistic MD simulations and dielectric relaxation spectroscopy measurements. The complementarity of the simulation and experimental techniques allows the exploration of the dynamics of polymer chains in the hybrid systems across a broad range of molecular weights and different size of nanoparticles. Experiments refer to systems with high MW PEO and larger nanoparticles, whereas simulations consider model systems of relatively short PEO chains and small nanoparticles. All together our systems also span a range of different chain confinement as shown in Table 1 . Moreover, the ratio of the size of polymer chains,  $R_g$ , over the radius of the nanoparticles,  $R$ , is rather similar for both experimental and model systems, i.e.  $R_g/R \sim 1-2$ . The main findings of the present work can be summarized as following:

Atomistic simulations reveal clear density heterogeneities in the model nanocomposites in the vicinity of the PEO/SiO<sub>2</sub> interface. A rather similar peak at a radial distance about 3-4 Å from the outer surface of the silica nanoparticles is observed for all three simulated systems denoting the attraction between the PEO<sub>49</sub> chains and the NP<sub>2</sub>. From the 3D density analysis, it is clear that, even for the most confined system investigated computationally, a considerable amount of polymeric material exists at the corners of the simulation domain, where the effect of the nanoparticle on its properties is attenuated.

A strong slowing down of the segmental dynamics is observed computationally in the adsorption layer that extends up to ~0.5nm from the outer surface of the nanoparticle, at the high-temperature regime. As the volume fraction of nanoparticles increases, a clear retardation of the segmental dynamics for all PEO chains is also observed.

On the other hand, the dynamics in nanohybrids composed of a high molecular weight PEO and silica nanoparticles, PEO<sub>2270</sub>/NP<sub>7</sub>, in different compositions was investigated experimentally utilizing Dielectric Relaxation Spectroscopy over the temperature range between far below the neat polymer glass transition up to below the polymer melting temperature. Two relaxation processes can be clearly resolved in all materials, one at low temperatures that is correlated with the local β-relaxation due to the motion of small groups in the chain and a second one above the T<sub>g</sub> of the bulk PEO<sub>2270</sub>, which is attributed to the segmental relaxation process. In all cases, and for both relaxation processes, no significant difference was observed between the dynamics of the neat polymer and its respective dynamics in the nanocomposites, despite the induced chain confinement. However, a closer look on the temperature dependence of the relaxation times indicates that, a more Arrhenius temperature dependence may be observed in the nanohybrids in contrast to the VFT dependence of the neat PEO<sub>2270</sub>. However, the temperature regime over which the α-relaxation can be observed is rather limited to extract safely such a conclusion. Overall, the experimental results obtained for the PEO<sub>2270</sub>/NP<sub>7</sub> nanohybrids seem to deviate from the behavior obtained for the same polymer when the chains were subjected in a two-dimensional confinement<sup>27</sup> as well from the results obtained computationally in the current work.

Figure 13 shows a combined Arrhenius representation of the relaxations times obtained for all different systems both experimentally and computationally in order to obtain a complementary picture of the dynamical behavior observed in the present work. Of course it is understood that

the simulated and the experimentally used PEO homopolymer exhibit different glass transition temperatures because of their different molecular weight. Superposition of the experimental and computational results show that the obtained differences are not that important and may be understood if the different available temperature regimes are considered in conjunction with the different temperature dependence of the segmental dynamics. It is noted again that, in the simulations, the probed temperature range is between  $T_g+100$  and  $T_g+150^\circ$  whereas, in the experiment, the segmental dynamics is observed between  $T_g$  and  $T_g +50^\circ$ .

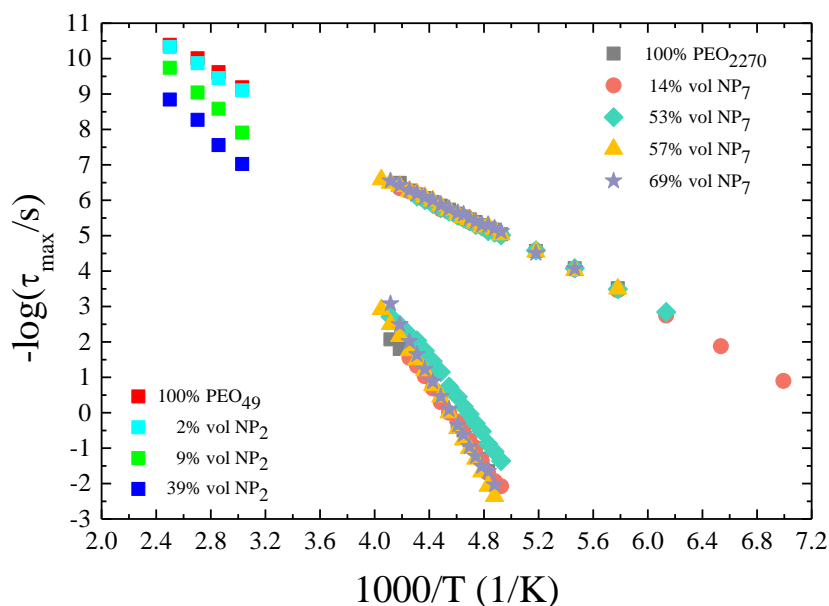


**Figure 13.** Arrhenius relaxation map for the neat PEO<sub>2270</sub> and PEO<sub>49</sub> and for the nanocomposites PEO<sub>2270</sub>/NP<sub>7</sub> PEO<sub>49</sub>/NP<sub>2</sub>.

Something that should also be considered is that, in the experiment, a high molecular weight polymer was utilized with a size that is approximately twice the radius of the nanoparticle, whereas, in the simulations, a polymer with a significantly smaller molecular weight was used with a size very close to the radius of the nanoparticle NP<sub>2</sub>. Therefore, in the former case, a large part of the chain can be extended away of the surface whereas in the latter the polymer segments have the ability to adsorb to a larger extent and, thus, their motion may be slower. Moreover, NMR experiments<sup>96</sup> showed the existence of a reduced-mobility layer in PEO/silica nanocomposites. Taking this into account, there is a strong possibility that the dynamics in such

a layer can be too slow to be detected by Dielectric Relaxation Spectroscopy giving rise only to the bulk-like dynamics of the chains away of the surface.

Last, when one compares results obtained by complementary techniques / methods, the particular specificities of each method that could lead to differences in the measured quantities should be always kept in mind. In the current case, one should consider that the perfect cubic arrangement of the nanoparticles assumed in the simulations is not very probable in real systems, where a rather random arrangement is anticipated and/or that PEO<sub>2270</sub> is a semi-crystalline polymer in contrast to PEO<sub>49</sub> that is purely amorphous. The former leads to a higher concentration of polymer/nanoparticle interfaces in the model systems, whereas, the amorphous/crystalline interfaces that exist in the experimental samples may lead to a different dynamical behavior of the PEO chains. Finally, as far as the atomistic model systems are concerned, one should note that for the PEO and the SiO<sub>2</sub> nanoparticle the atomistic models are well tested and used extensively in the literature<sup>93,101</sup>; however, for the polymer-nanoparticle interactions, typical mixing (Lorentz-Berthelot) rules were used, which might not describe accurately enough the complex PEO-SiO<sub>2</sub> interaction.<sup>108,109</sup>

All the above are, naturally, potential directions of future work. Overall, despite the observed differences the complementarity of the detailed atomistic simulations and dielectric relaxation experiments offer a direct way to probe the dynamics of PEO chains in PEO/SiO<sub>2</sub> systems across a broad range of molecular weights, volume concentrations of nanoparticles and temperatures that is not accessible by one technique alone.

## ASSOCIATED CONTENT

### Supporting Information.

<sup>1</sup>Video from our MD simulation of hybrid polyethylene oxide/silica nanoparticle at 400 K. The PEO<sub>49</sub> chains are shown green and the SiO<sub>2</sub> NP<sub>2</sub> red. (MP4)

<sup>2</sup>Video representation of the PEO<sub>49</sub> 3D density profiles in the PEO/SiO<sub>2</sub> system with  $\phi_{\text{NP}} = 19\%$  at 400 K. Different slices, of 3.2 Å thickness, parallel to the  $xy$  plane are used at various distances from the center of the SiO<sub>2</sub> nanoparticle. (3D-Density-Profile-PEO-SilicaNP.MP4)

<sup>3</sup>The autocorrelation functions  $C_{\text{ads}}$  of the adsorption state S of the PEO atoms for all temperatures and for the systems with concentration of: (a)  $\phi_{\text{NP}} = 2\%$ ; (b)  $\phi_{\text{NP}} = 19\%$ ; (c)  $\phi_{\text{NP}} = 39\%$ . (PDF)

## **AUTHOR INFORMATION**

### **Corresponding Author**

\*Kiriaki Chrissopoulou, Institute of Electronic Structure and Laser, Foundation for Research and Technology-Hellas, 700 13 Heraklion Crete, Greece

\*Vagelis Harmandaris, Department of Mathematics & Applied Mathematics, University of Crete, 70013 Heraklion Crete, Greece and Institute of Applied and Computational Mathematics, Foundation for Research and Technology-Hellas, 700 13 Heraklion Crete, Greece and Computation-based Science and Technology Research Center, The Cyprus Institute, 2121 Nicosia, Cyprus

\*Spiros H. Anastasiadis, Institute of Electronic Structure and Laser, Foundation for Research and Technology-Hellas, 700 13 Heraklion Crete, Greece and Department of Chemistry, University of Crete, P.O. Box 2208, 710 03 Heraklion Crete, Greece

### **Present Addresses**

Hellen Papapanou, NSF BioPACIFIC Materials Innovation Platform (MIP), Santa Barbara, CA, USA.

### **Author Contributions**

The manuscript was written through contributions of all authors. All authors have given approval to the final version of the manuscript. ‡These authors contributed equally. (match statement to author names with a symbol)

### **Notes**

Any additional relevant notes should be placed here.

## **ACKNOWLEDGMENT**

This research has been partially supported by the project “National Research Infrastructure on nanotechnology, advanced materials and micro/nanoelectronics” (MIS 5002772) implemented

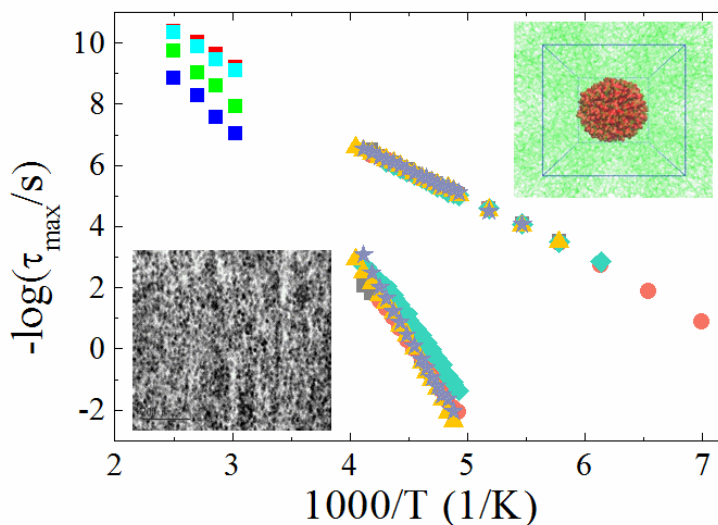
under the “Action for the Strategic Development on the Research and Technological Sector”, funded by the Operational Programme "Competitiveness, Entrepreneurship and Innovation" (NSRF 2014-2020). We acknowledge Manolis Doxastakis and Yogendra Pandey for sharing with us the model silica configurations. AR and VH acknowledge support by project “SimEA”, funded by the European Union’s Horizon 2020 research and innovation programme under Grant Agreement No. 810660. The work was supported by computational time granted from the Greek Research & Technology Network (GRNET) in the National HPC facility ARIS under a project named POL-COMP-TIRE.

Finally, we would like to thank Doros Theodorou for several years of fruitful collaborations and scientific discussions.

## ABBREVIATIONS

PNCs, polymer nanocomposites; MD, molecular dynamics; DRS, dielectric relaxation spectroscopy.

## TOC



## REFERENCES

- (1) Bailey, E. J.; Winey, K. I. Dynamics of polymer segments, polymer chains, and nanoparticles in polymer nanocomposite melts: A review. *Progress in Polymer Science* **2020**, *105*, 101242.
- (2) Richter, D.; Kruteva, M. Polymer dynamics under confinement. *Soft Matter* **2019**, *15*, 7316-7349.
- (3) Karatrantos, A.; Composto, R. J.; Winey, K. I.; Kröger, M.; Clarke, N. Modeling of Entangled Polymer Diffusion in Melts and Nanocomposites: A Review. *Polymers* **2019**, *11*.
- (4) Vogiatzis, G. G.; Theodorou, D. N. Multiscale Molecular Simulations of Polymer-Matrix Nanocomposites. *Archives of Computational Methods in Engineering* **2018**, *25*, 591-645.
- (5) Mallakpour, S.; Naghdi, M. Polymer/SiO<sub>2</sub> nanocomposites: Production and applications. *Progress in Materials Science* **2018**, *97*, 409-447.
- (6) Müller, K.; Bugnicourt, E.; Latorre, M.; Jorda, M.; Echegoyen Sanz, Y.; Lagaron, J. M.; Miesbauer, O.; Bianchin, A.; Hankin, S.; Bölz, U.; Pérez, G.; Jesdinszki, M.; Lindner, M.; Scheuerer, Z.; Castelló, S.; Schmid, M. Review on the Processing and Properties of Polymer Nanocomposites and Nanocoatings and Their Applications in the Packaging, Automotive and Solar Energy Fields. *Nanomaterials* **2017**, *7*.
- (7) Zou, H.; Wu, S.; Shen, J. Polymer/Silica Nanocomposites: Preparation, Characterization, Properties, and Applications. *Chemical Reviews* **2008**, *108*, 3893-3957.
- (8) Hegde, M.; Yang, L.; Vita, F.; Fox, R. J.; van de Watering, R.; Norder, B.; Lafont, U.; Francescangeli, O.; Madsen, L. A.; Picken, S. J.; Samulski, E. T.; Dingemans, T. J. Strong graphene oxide nanocomposites from aqueous hybrid liquid crystals. *Nature Communications* **2020**, *11*, 830.
- (9) Koh, C.; Grest, G. S. Assembly of Polymer-Grafted Nanoparticles in Polymer Matrices. **2020**, *14*, 13491-13499.
- (10) Kinloch, I. A.; Suhr, J. Composites with carbon nanotubes and graphene: An outlook. **2018**, *362*, 547-553.
- (11) Jancar, J.; Douglas, J. F.; Starr, F. W.; Kumar, S. K.; Cassagnau, P.; Lesser, A. J.; Sternstein, S. S.; Buehler, M. J. Current issues in research on structure–property relationships in polymer nanocomposites. *Polymer* **2010**, *51*, 3321-3343.
- (12) Feldman, D. Polymers and Polymer Nanocomposites for Cancer Therapy. *Applied Sciences* **2019**, *9*.
- (13) Rissanou, A. N.; Papananou, H.; Petrakis, V. S.; Doxastakis, M.; Andrikopoulos, K. S.; Voyiatzis, G. A.; Chrissopoulou, K.; Harmandaris, V.; Anastasiadis, S. H. Structural and Conformational Properties of Poly(ethylene oxide)/Silica Nanocomposites: Effect of Confinement. *Macromolecules* **2017**, *50*, 6273-6284.
- (14) Bačová, P.; Li, W.; Behbahani, A. F.; Burkhart, C.; Polińska, P.; Doxastakis, M.; Harmandaris, V. Coupling between Polymer Conformations and Dynamics Near Amorphous Silica Surfaces: A Direct Insight from Atomistic Simulations. *Nanomaterials* **2021**, *11*.
- (15) Behbahani, A. F.; Rissanou, A.; Kritikos, G.; Doxastakis, M.; Burkhart, C.; Polińska, P.; Harmandaris, V. A. Conformations and Dynamics of Polymer Chains in Cis and Trans Polybutadiene/Silica Nanocomposites through Atomistic Simulations: From the Unentangled to the Entangled Regime. *Macromolecules* **2020**, *53*, 6173-6189.
- (16) Baeza, G. P.; Dessi, C.; Costanzo, S.; Zhao, D.; Gong, S.; Alegria, A.; Colby, R. H.; Rubinstein, M.; Vlassopoulos, D.; Kumar, S. K. Network dynamics in nanofilled polymers. *Nature Communications* **2016**, *7*, 11368.

- (17) Papananou, H.; Perivolari, E.; Chrissopoulou, K.; Anastasiadis, S. H. Tuning polymer crystallinity via the appropriate selection of inorganic nanoadditives. *Polymer* **2018**, *157*, 111-121.
- (18) Chrissopoulou, K.; Andrikopoulos, K. S.; Fotiadou, S.; Bollas, S.; Karageorgaki, C.; Christofilos, D.; Voyiatzis, G. A.; Anastasiadis, S. H. Crystallinity and Chain Conformation in PEO/Layered Silicate Nanocomposites. *Macromolecules* **2011**, *44*, 9710-9722.
- (19) Michell, R. M.; Müller, A. J. Confined crystallization of polymeric materials. *Progress in Polymer Science* **2016**, *54-55*, 183-213.
- (20) Sangroniz, L.; van Drongelen, M.; Cardinaels, R.; Santamaria, A.; Peters, G. W. M.; Müller, A. J. Effect of shear rate and pressure on the crystallization of PP nanocomposites and PP/PET polymer blend nanocomposites. *Polymer* **2020**, *186*, 121950.
- (21) Bollas, S.; Chrissopoulou, K.; Andrikopoulos, K. S.; Voyiatzis, G. A.; Anastasiadis, S. H. Polymer Conformation under Confinement. *Polymers* **2017**, *9*.
- (22) Carr, J. M.; Langhe, D. S.; Ponting, M. T.; Hiltner, A.; Baer, E. Confined crystallization in polymer nanolayered films: A review. *Journal of Materials Research* **2012**, *27*, 1326-1350.
- (23) Barroso-Bujans, F.; Cervený, S.; Alegría, Á.; Colmenero, J. Chain Length Effects on the Dynamics of Poly(ethylene oxide) Confined in Graphite Oxide: A Broadband Dielectric Spectroscopy Study. *Macromolecules* **2013**, *46*, 7932-7939.
- (24) Panagopoulou, A.; Rodríguez-Tinoco, C.; White, R. P.; Lipson, J. E. G.; Napolitano, S. Substrate Roughness Speeds Up Segmental Dynamics of Thin Polymer Films. *Physical Review Letters* **2020**, *124*, 027802.
- (25) Androulaki, K.; Chrissopoulou, K.; Prevosto, D.; Labardi, M.; Anastasiadis, S. H. Dynamics of Hyperbranched Polymers under Confinement: A Dielectric Relaxation Study. *ACS Applied Materials & Interfaces* **2015**, *7*, 12387-12398.
- (26) Chrissopoulou, K.; Fotiadou, S.; Frick, B.; Anastasiadis, S. H. Structure and Dynamics in Hydrophilic Polymer/Layered Silicate Nanocomposites. *Macromolecular Symposia* **2013**, *331-332*, 50-57.
- (27) Elmahdy, M. M.; Chrissopoulou, K.; Afratis, A.; Floudas, G.; Anastasiadis, S. H. Effect of Confinement on Polymer Segmental Motion and Ion Mobility in PEO/Layered Silicate Nanocomposites. *Macromolecules* **2006**, *39*, 5170-5173.
- (28) Shah, S.; Famta, P.; Raghuvanshi, R. S.; Singh, S. B.; Srivastava, S. Lipid polymer hybrid nanocarriers: Insights into synthesis aspects, characterization, release mechanisms, surface functionalization and potential implications. *Colloid and Interface Science Communications* **2022**, *46*, 100570.
- (29) Han, J.; Zhao, D.; Li, D.; Wang, X.; Jin, Z.; Zhao, K. Polymer-Based Nanomaterials and Applications for Vaccines and Drugs. *Polymers* **2018**, *10*, 31.
- (30) Fortuni, B.; Inose, T.; Ricci, M.; Fujita, Y.; Van Zundert, I.; Masuhara, A.; Fron, E.; Mizuno, H.; Latterini, L.; Rocha, S.; Uji-i, H. Polymeric Engineering of Nanoparticles for Highly Efficient Multifunctional Drug Delivery Systems. *Scientific Reports* **2019**, *9*, 2666.
- (31) Mathioudakis, I. G.; Vogiatzis, G. G.; Tzoumanekas, C.; Theodorou, D. N. Multiscale simulations of PS–SiO<sub>2</sub> nanocomposites: from melt to glassy state. *Soft Matter* **2016**, *12*, 7585-7605.
- (32) Hong, B.; Chremos, A.; Panagiotopoulos, A. Z. Dynamics in coarse-grained models for oligomer-grafted silica nanoparticles. *The Journal of Chemical Physics* **2012**, *136*, 204904.

- (33) Rissanou, A. N.; Power, A. J.; Harmandaris, V. Structural and Dynamical Properties of Polyethylene/Graphene Nanocomposites through Molecular Dynamics Simulations. *Polymers* **2015**, *7*, 390-417.
- (34) Power, A. J.; Remediakis, I. N.; Harmandaris, V. Interface and Interphase in Polymer Nanocomposites with Bare and Core-Shell Gold Nanoparticles. *Polymers* **2021**, *13*, 541.
- (35) Nodoro, T. V. M.; Voyiatzis, E.; Ghanbari, A.; Theodorou, D. N.; Böhm, M. C.; Müller-Plathe, F. Interface of Grafted and Ungrafted Silica Nanoparticles with a Polystyrene Matrix: Atomistic Molecular Dynamics Simulations. *Macromolecules* **2011**, *44*, 2316-2327.
- (36) Nodoro, T. V. M.; Böhm, M. C.; Müller-Plathe, F. Interface and Interphase Dynamics of Polystyrene Chains near Grafted and Ungrafted Silica Nanoparticles. *Macromolecules* **2012**, *45*, 171-179.
- (37) Voyiatzis, G. G.; Theodorou, D. N. Local Segmental Dynamics and Stresses in Polystyrene-C60 Mixtures. *Macromolecules* **2014**, *47*, 387-404.
- (38) Skountzos, E. N.; Anastassiou, A.; Mavrantzas, V. G.; Theodorou, D. N. Determination of the Mechanical Properties of a Poly(methyl methacrylate) Nanocomposite with Functionalized Graphene Sheets through Detailed Atomistic Simulations. *Macromolecules* **2014**, *47*, 8072-8088.
- (39) Rissanou, A. N.; Bačová, P.; Harmandaris, V. Investigation of the properties of nanographene in polymer nanocomposites through molecular simulations: dynamics and anisotropic Brownian motion. *Physical Chemistry Chemical Physics* **2019**, *21*, 23843-23854.
- (40) Pandey, Y. N.; Papakonstantopoulos, G. J.; Doxastakis, M. Polymer/Nanoparticle Interactions: Bridging the Gap. *Macromolecules* **2013**, *46*, 5097-5106.
- (41) Roussou, R.-E.; Karatasos, K. Graphene/poly(ethylene glycol) nanocomposites as studied by molecular dynamics simulations. *Materials & Design* **2016**, *97*, 163-174.
- (42) Zhou, M.; Liu, J.; Hou, G.; Yang, H.; Zhang, L. Study on structures, dynamics and mechanical properties of styrene butadiene rubber (SBR)/silica interfaces: A fully atomistic molecular dynamics. *Polymer* **2021**, *218*, 123523.
- (43) Brown, D.; Marcadon, V.; Mélé, P.; Albérola, N. D. Effect of Filler Particle Size on the Properties of Model Nanocomposites. *Macromolecules* **2008**, *41*, 1499-1511.
- (44) Kalathi, J. T.; Kumar, S. K.; Rubinstein, M.; Grest, G. S. Rouse mode analysis of chain relaxation in polymer nanocomposites. *Soft Matter* **2015**, *11*, 4123-4132.
- (45) Li, Y.; Kröger, M.; Liu, W. K. Nanoparticle Effect on the Dynamics of Polymer Chains and Their Entanglement Network. *Physical Review Letters* **2012**, *109*, 118001.
- (46) Zhang, W.; Emamy, H.; Pazmiño Betancourt, B. A.; Vargas-Lara, F.; Starr, F. W.; Douglas, J. F. The interfacial zone in thin polymer films and around nanoparticles in polymer nanocomposites. *The Journal of Chemical Physics* **2019**, *151*, 124705.
- (47) Skountzos, E. N.; Tsalikis, D. G.; Stephanou, P. S.; Mavrantzas, V. G. Individual Contributions of Adsorbed and Free Chains to Microscopic Dynamics of Unentangled poly(ethylene Glycol)/Silica Nanocomposite Melts and the Important Role of End Groups: Theory and Simulation. *Macromolecules* **2021**, *54*, 4470-4487.
- (48) Barbier, D.; Brown, D.; Grillet, A.-C.; Neyertz, S. Interface between End-Functionalized PEO Oligomers and a Silica Nanoparticle Studied by Molecular Dynamics Simulations. *Macromolecules* **2004**, *37*, 4695-4710.

- (49) Glomann, T.; Schneider, G. J.; Allgaier, J.; Radulescu, A.; Lohstroh, W.; Farago, B.; Richter, D. Microscopic Dynamics of Polyethylene Glycol Chains Interacting with Silica Nanoparticles. *Physical Review Letters* **2013**, *110*, 178001.
- (50) Cheng, S.; Carroll, B.; Lu, W.; Fan, F.; Carrillo, J.-M. Y.; Martin, H.; Holt, A. P.; Kang, N.-G.; Bocharova, V.; Mays, J. W.; Sumpter, B. G.; Dadmun, M.; Sokolov, A. P. Interfacial Properties of Polymer Nanocomposites: Role of Chain Rigidity and Dynamic Heterogeneity Length Scale. *Macromolecules* **2017**, *50*, 2397-2406.
- (51) Füllbrandt, M.; Purohit, P. J.; Schönhals, A. Combined FTIR and Dielectric Investigation of Poly(vinyl acetate) Adsorbed on Silica Particles. *Macromolecules* **2013**, *46*, 4626-4632.
- (52) Gong, S.; Chen, Q.; Moll, J. F.; Kumar, S. K.; Colby, R. H. Segmental Dynamics of Polymer Melts with Spherical Nanoparticles. *ACS Macro Letters* **2014**, *3*, 773-777.
- (53) Senses, E.; Faraone, A.; Akcora, P. Microscopic Chain Motion in Polymer Nanocomposites with Dynamically Asymmetric Interphases. *Scientific Reports* **2016**, *6*, 29326.
- (54) Harton, S. E.; Kumar, S. K.; Yang, H.; Koga, T.; Hicks, K.; Lee, H.; Mijovic, J.; Liu, M.; Vallery, R. S.; Gidley, D. W. Immobilized Polymer Layers on Spherical Nanoparticles. *Macromolecules* **2010**, *43*, 3415-3421.
- (55) Cheng, S.; Xie, S.-J.; Carrillo, J.-M. Y.; Carroll, B.; Martin, H.; Cao, P.-F.; Dadmun, M. D.; Sumpter, B. G.; Novikov, V. N.; Schweizer, K. S.; Sokolov, A. P. Big Effect of Small Nanoparticles: A Shift in Paradigm for Polymer Nanocomposites. *ACS Nano* **2017**, *11*, 752-759.
- (56) Hocken, A.; Beyer, F. L.; Lee, J. S.; Grim, B. J.; Mithaiwala, H.; Green, M. D. Covalently integrated silica nanoparticles in poly(ethylene glycol)-based acrylate resins: thermomechanical, swelling, and morphological behavior. *Soft Matter* **2022**, *18*, 1019-1033.
- (57) Senses, E.; Darvishi, S.; Tyagi, M. S.; Faraone, A. Entangled Polymer Dynamics in Attractive Nanocomposite Melts. *Macromolecules* **2020**, *53*, 4982-4989.
- (58) Androulaki, K.; Chrissopoulou, K.; Labardi, M.; Anastasiadis, S. H. Effect of interfacial interactions on static and dynamic behavior of hyperbranched polymers: Comparison between different layered nanoadditives. *Polymer* **2021**, *222*, 123646.
- (59) Chrissopoulou, K.; Androulaki, K.; Labardi, M.; Anastasiadis, S. H. Static and Dynamic Behavior of Polymer/Graphite Oxide Nanocomposites before and after Thermal Reduction. *Polymers* **2021**, *13*.
- (60) Fotiadou, S.; Karageorgaki, C.; Chrissopoulou, K.; Karatasos, K.; Tanis, I.; Tragoudaras, D.; Frick, B.; Anastasiadis, S. H. Structure and Dynamics of Hyperbranched Polymer/Layered Silicate Nanocomposites. *Macromolecules* **2013**, *46*, 2842-2855.
- (61) Holt, A. P.; Griffin, P. J.; Bocharova, V.; Agapov, A. L.; Imel, A. E.; Dadmun, M. D.; Sangoro, J. R.; Sokolov, A. P. Dynamics at the Polymer/Nanoparticle Interface in Poly(2-vinylpyridine)/Silica Nanocomposites. *Macromolecules* **2014**, *47*, 1837-1843.
- (62) Klonos, P.; Kulyk, K.; Borysenko, M. V.; Gun'ko, V. M.; Kyritsis, A.; Pissis, P. Effects of Molecular Weight below the Entanglement Threshold on Interfacial Nanoparticles/Polymer Dynamics. *Macromolecules* **2016**, *49*, 9457-9473.
- (63) Oh, S. M.; Abbasi, M.; Shin, T. J.; Saalwächter, K.; Kim, S. Y. Initial Solvent-Driven Nonequilibrium Effect on Structure, Properties, and Dynamics of Polymer Nanocomposites. *Physical Review Letters* **2019**, *123*, 167801.

- (64) Bogoslovov, R. B.; Roland, C. M.; Ellis, A. R.; Randall, A. M.; Robertson, C. G. Effect of Silica Nanoparticles on the Local Segmental Dynamics in Poly(vinyl acetate). *Macromolecules* **2008**, *41*, 1289-1296.
- (65) Salahshoori, I.; Seyfaee, A.; Babapoor, A.; Neville, F.; Moreno-Atanasio, R. Evaluation of the effect of silica nanoparticles, temperature and pressure on the performance of PSF/PEG/SiO<sub>2</sub> mixed matrix membranes: A molecular dynamics simulation (MD) and design of experiments (DOE) study. *Journal of Molecular Liquids* **2021**, *333*, 115957.
- (66) Yang, S.-A.; Choi, S.; Jeon, S. M.; Yu, J. Silica nanoparticle stability in biological media revisited. *Scientific Reports* **2018**, *8*, 185.
- (67) Chen, F.; Ma, K.; Madajewski, B.; Zhuang, L.; Zhang, L.; Rickert, K.; Marelli, M.; Yoo, B.; Turker, M. Z.; Overholtzer, M.; Quinn, T. P.; Gonen, M.; Zanzonico, P.; Tuesca, A.; Bowen, M. A.; Norton, L.; Subramony, J. A.; Wiesner, U.; Bradbury, M. S. Ultrasmall targeted nanoparticles with engineered antibody fragments for imaging detection of HER2-overexpressing breast cancer. *Nature Communications* **2018**, *9*, 4141.
- (68) Bharti, C.; Nagaich, U.; Pal, A. K.; Gulati, N. Mesoporous silica nanoparticles in target drug delivery system: A review. *Int J Pharm Investig* **2015**, *5*, 124-133.
- (69) Foglia, S.; Ledda, M.; Fioretti, D.; Iucci, G.; Papi, M.; Capellini, G.; Lolli, M. G.; Grimaldi, S.; Rinaldi, M.; Lisi, A. In vitro biocompatibility study of sub-5 nm silica-coated magnetic iron oxide fluorescent nanoparticles for potential biomedical application. *Scientific Reports* **2017**, *7*, 46513.
- (70) Meng, F.; Elshahati, M.; Liu, J.; Richards, R. F. Thermal resistance between amorphous silica nanoparticles. *Journal of Applied Physics* **2017**, *121*, 194302.
- (71) Chen, L.; Liu, J.; Zhang, Y.; Zhang, G.; Kang, Y.; Chen, A.; Feng, X.; Shao, L. The toxicity of silica nanoparticles to the immune system. *Nanomedicine* **2018**, *13*, 1939-1962.
- (72) Purcar, V.; Rădițoiu, V.; Nichita, C.; Bălan, A.; Rădițoiu, A.; Căprărescu, S.; Raduly, F. M.; Manea, R.; Șomoghi, R.; Nicolae, C.-A.; Raut, I.; Jecu, L. Preparation and Characterization of Silica Nanoparticles and of Silica-Gentamicin Nanostructured Solution Obtained by Microwave-Assisted Synthesis. *Materials* **2021**, *14*.
- (73) Abburi, A.; Ali, M.; Moriya, P. V. Synthesis of mesoporous silica nanoparticles from waste hexafluorosilicic acid of fertilizer industry. *Journal of Materials Research and Technology* **2020**, *9*, 8074-8080.
- (74) Li, H.; Chen, X.; Shen, D.; Wu, F.; Pleixats, R.; Pan, J. Functionalized silica nanoparticles: classification, synthetic approaches and recent advances in adsorption applications. *Nanoscale* **2021**, *13*, 15998-16016.
- (75) Gao, Y.; Wang, Y.; Fu, A.; Shi, W.; Yeo, D.; Luo, K. Q.; Ow, H.; Xu, C. Tracking mesenchymal stem cell tumor-homing using fluorescent silica nanoparticles. *Journal of Materials Chemistry B* **2015**, *3*, 1245-1253.
- (76) Mathelié-Guinlet, M.; Cohen-Bouhacina, T.; Gammoudi, I.; Martin, A.; Béven, L.; Delville, M.-H.; Grauby-Heywang, C. Silica nanoparticles-assisted electrochemical biosensor for the rapid, sensitive and specific detection of Escherichia coli. *Sensors and Actuators B: Chemical* **2019**, *292*, 314-320.
- (77) Jafari, S.; Derakhshankhah, H.; Alaei, L.; Fattahi, A.; Varnamkhasti, B. S.; Saboury, A. A. Mesoporous silica nanoparticles for therapeutic/diagnostic applications. *Biomedicine & Pharmacotherapy* **2019**, *109*, 1100-1111.
- (78) Miyata, T.; Nagao, T.; Watanabe, D.; Kumagai, A.; Akutagawa, K.; Morita, H.; Jinnai, H. Nanoscale Stress Distribution in Silica-Nanoparticle-Filled Rubber as Observed by

Transmission Electron Microscopy: Implications for Tire Application. *ACS Applied Nano Materials* **2021**, *4*, 4452-4461.

(79) Upadhye, S. B.; Rajabi-Siahboomi, A. R.: Properties and Applications of Polyethylene Oxide and Ethylcellulose for Tamper Resistance and Controlled Drug Delivery. In *Melt Extrusion: Materials, Technology and Drug Product Design*; Repka, M. A., Langley, N., DiNunzio, J., Eds.; Springer New York: New York, NY, 2013; pp 145-158.

(80) Teran, A. A.; Tang, M. H.; Mullin, S. A.; Balsara, N. P. Effect of molecular weight on conductivity of polymer electrolytes. *Solid State Ionics* **2011**, *203*, 18-21.

(81) Fan, X.; Hu, Z.; Wang, G. Synthesis and unimolecular micelles of amphiphilic copolymer with dendritic poly(l-lactide) core and poly(ethylene oxide) shell for drug delivery. *RSC Advances* **2015**, *5*, 100816-100823.

(82) Tang, Z.; He, C.; Tian, H.; Ding, J.; Hsiao, B. S.; Chu, B.; Chen, X. Polymeric nanostructured materials for biomedical applications. *Progress in Polymer Science* **2016**, *60*, 86-128.

(83) Glynos, E.; Papoutsakis, L.; Pan, W.; Giannelis, E. P.; Nega, A. D.; Mygiakis, E.; Sakellariou, G.; Anastasiadis, S. H. Nanostructured Polymer Particles as Additives for High Conductivity, High Modulus Solid Polymer Electrolytes. *Macromolecules* **2017**, *50*, 4699-4706.

(84) Glynos, E.; Petropoulou, P.; Mygiakis, E.; Nega, A. D.; Pan, W.; Papoutsakis, L.; Giannelis, E. P.; Sakellariou, G.; Anastasiadis, S. H. Leveraging Molecular Architecture To Design New, All-Polymer Solid Electrolytes with Simultaneous Enhancement in Modulus and Ionic Conductivity. *Macromolecules* **2018**, *51*, 2542-2550.

(85) Homann, G.; Stolz, L.; Nair, J.; Laskovic, I. C.; Winter, M.; Kasnatscheew, J. Poly(Ethylene Oxide)-based Electrolyte for Solid-State-Lithium-Batteries with High Voltage Positive Electrodes: Evaluating the Role of Electrolyte Oxidation in Rapid Cell Failure. *Scientific Reports* **2020**, *10*, 4390.

(86) Philippova, O. E.; Kuchanov, S. I.; Topchieva, I. N.; Kabanov, V. A. Hydrogen bonds in dilute solutions of poly(ethylene glycol). *Macromolecules* **1985**, *18*, 1628-1633.

(87) Cao, Y.; Guan, Y.; Du, J.; Luo, J.; Peng, Y.; Yip, C. W.; Chan, A. S. C. Hydrogen-bonded polymer network—poly(ethylene glycol) complexes with shape memory effect. *Journal of Materials Chemistry* **2002**, *12*, 2957-2960.

(88) Kozłowska, M.; Goclon, J.; Rodziewicz, P. Intramolecular Hydrogen Bonds in Low-Molecular-Weight Polyethylene Glycol. *Chemphyschem : a European journal of chemical physics and physical chemistry* **2016**, *17*, 1143-1153.

(89) Ma, L.; Deng, L.; Chen, J. Applications of poly(ethylene oxide) in controlled release tablet systems: a review. *Drug development and industrial pharmacy* **2014**, *40*, 845-851.

(90) Zhang, Q.; Archer, L. A. Poly(ethylene oxide)/Silica Nanocomposites: Structure and Rheology. *Langmuir* **2002**, *18*, 10435-10442.

(91) Issa, S.; Cousin, F.; Bonnevide, M.; Gigmès, D.; Jestin, J.; Phan, T. N. T. Poly(ethylene oxide) grafted silica nanoparticles: efficient routes of synthesis with associated colloidal stability. *Soft Matter* **2021**, *17*, 6552-6565.

(92) Li, B.; Shu, D.; Wang, R.; Zhai, L.; Chai, Y.; Lan, Y.; Cao, H.; Zou, C. Polyethylene glycol/silica (PEG@SiO<sub>2</sub>) composite inspired by the synthesis of mesoporous materials as shape-stabilized phase change material for energy storage. *Renewable Energy* **2020**, *145*, 84-92.

- (93) Hong, B.; Panagiotopoulos, A. Z. Molecular Dynamics Simulations of Silica Nanoparticles Grafted with Poly(ethylene oxide) Oligomer Chains. *The Journal of Physical Chemistry B* **2012**, *116*, 2385-2395.
- (94) Golitsyn, Y.; Schneider, G. J.; Saalwächter, K. Reduced-mobility layers with high internal mobility in poly(ethylene oxide)–silica nanocomposites. *The Journal of Chemical Physics* **2017**, *146*, 203303.
- (95) Glomann, T.; Hamm, A.; Allgaier, J.; Hübner, E. G.; Radulescu, A.; Farago, B.; Schneider, G. J. A microscopic view on the large scale chain dynamics in nanocomposites with attractive interactions. *Soft Matter* **2013**, *9*, 10559-10571.
- (96) Kim, S. Y.; Meyer, H. W.; Saalwächter, K.; Zukoski, C. F. Polymer Dynamics in PEG-Silica Nanocomposites: Effects of Polymer Molecular Weight, Temperature and Solvent Dilution. *Macromolecules* **2012**, *45*, 4225-4237.
- (97) Lorthioir, C.; Lauprêtre, F.; Soulestin, J.; Lefebvre, J.-M. Segmental Dynamics of Poly(ethylene oxide) Chains in a Model Polymer/Clay Intercalated Phase: Solid-State NMR Investigation. *Macromolecules* **2009**, *42*, 218-230.
- (98) Lagrené, K.; Zanotti, J. M.; Daoud, M.; Farago, B.; Judeinstein, P. Dynamical behavior of a single polymer chain under nanometric confinement. *The European Physical Journal Special Topics* **2010**, *189*, 231-237.
- (99) *Physical Properties of Polymers Handbook*, 2007.
- (100) Tsamopoulos, A. J.; Katsarou, A. F.; Tsalikis, D. G.; Mavrantzas, V. G. Shear Rheology of Unentangled and Marginally Entangled Ring Polymer Melts from Large-Scale Nonequilibrium Molecular Dynamics Simulations. *Polymers* **2019**, *11*, 1194.
- (101) Fischer, J.; Paschek, D.; Geiger, A.; Sadowski, G. Modeling of Aqueous Poly(oxyethylene) Solutions: 1. Atomistic Simulations. *The Journal of Physical Chemistry B* **2008**, *112*, 2388-2398.
- (102) Pandey, Y. N.; Doxastakis, M. Detailed atomistic Monte Carlo simulations of a polymer melt on a solid surface and around a nanoparticle. *The Journal of Chemical Physics* **2012**, *136*, 094901.
- (103) Parrinello, M.; Rahman, A. Polymorphic transitions in single crystals: A new molecular dynamics method. *Journal of Applied Physics* **1981**, *52*, 7182-7190.
- (104) Hoover, W. G. Canonical dynamics: Equilibrium phase-space distributions. *Physical Review A* **1985**, *31*, 1695-1697.
- (105) Berendsen, H. J. C.; van der Spoel, D.; van Drunen, R. GROMACS: A message-passing parallel molecular dynamics implementation. *Computer Physics Communications* **1995**, *91*, 43-56.
- (106) Foroozani Behbahani, A.; Harmandaris, V. Gradient of Segmental Dynamics in Stereoregular Poly(methyl methacrylate) Melts Confined between Pristine or Oxidized Graphene Sheets. *Polymers* **2021**, *13*.
- (107) Kremer, F.; Schönhals, A.: *Broadband Dielectric Spectroscopy*. Springer Berlin Heidelberg, 2003.
- (108) Johnston, K.; Harmandaris, V. Properties of short polystyrene chains confined between two gold surfaces through a combined density functional theory and classical molecular dynamics approach. *Soft Matter* **2012**, *8*, 6320-6332.
- (109) Patsalidis, N.; Papamokos, G.; Floudas, G.; Harmandaris, V. Understanding the Interaction between Polybutadiene and Alumina via DFT Calculations and Machine-learned Atomistic Simulations. **2022**.

